Graduate School Form
30 Updated 12/26/2015

PURDUE UNIVERSITY
GRADUATE SCHOOL
Thesis/Dissertation Acceptance

This is to certify that the thesis/dissertation prepared

By Fabian Lischke

Entitled

Design of Self-supported 3D Printed Parts for Fused Deposition Modeling

For the degree of Master of Science in Mechanical Engineering

Is approved by the final examining committee:

Andres Tovar
Chair

Sohel Anwar

Alan Jones

To the best of my knowledge and as understood by the student in the Thesis/Dissertation Agreement, Publication Delay, and Certification Disclaimer (Graduate School Form 32), this thesis/dissertation adheres to the provisions of Purdue University's "Policy of Integrity in Research" and the use of copyright material.

Approved by Major Professor(s): Andres Tovar

Approved by: Sohel Anwar 4/20/2016

Head of the Departmental Graduate Program Date

DESIGN OF SELF-SUPPORTED 3D PRINTED PARTS FOR FUSED DEPOSITION MODELING

A Thesis

Submitted to the Faculty

of

Purdue University

by

Fabian Lischke

In Partial Fulfillment of the

Requirements for the Degree

of

Master of Science in Mechanical Engineering

May 2016

Purdue University

Indianapolis, Indiana

Dedicated to my family.

ACKNOWLEDGMENTS

Although my name is the only one featured on the title for this thesis, many people have devoted their time and effort to make the research successful. I thank everybody for their support and assistance to made this research possible.

I wish to thank my advisor, Dr. Andrés Tovar. With Dr. Tovar, I have been blessed to have an advisor, who gave me the freedom to explore the area of interest by myself but also guided me and was an excellent mentor in every situation. Dr. Tovar helped me understand how to challenge an idea and to get more out of it. With his guidance I was able to look outside the box and push the research forward. With his trust, Dr. Tovar gave me the confidence in every situation to finish this thesis.

During this research I was honored to work with Eduardo Salcedo. He is a undergraduate student in Motorsports Engineering and his interest and knowledge in 3D printing is outstanding. Eduardo was a great help in not only providing his 3D printer, the MakerBot Replicator 2X, but he also helped in the study of self-supported structures. The discussions I had with him, helped as an input for the tests and results in this study.

Last but not least, I want to say thank you to my family. It is hard to live in a new country by yourself. With the help and support of my family over the last two years I have overcome setbacks and stay focused on my graduate study. My family made it possible for me to gain my graduate experience at IUPUI and for that, I will cherish forever.

TABLE OF CONTENTS

Page

LIST OF TABLES vi

LIST OF FIGURES vii

ABSTRACT xii

1. INTRODUCTION 1
   1.1 Motivation 1
   1.2 State of the Art in Design for Additive Manufacturing 2
   1.3 Research Gap in Simulation-based Design for Additive Manufacturing 6
   1.4 Objective 7
   1.5 Research Approach 8

2. ANALYTIC MODEL OF EXTRUDED FILAMENT 9
   2.1 Fused Deposition Modeling Process 9
   2.2 Design Formulation 12
      2.2.1 Euler-Bernoulli Beam Theory 14
      2.2.2 Timoshenko's Modified Beam Theory 16
   2.3 Summary 20

3. PHYSICAL TESTING 21
   3.1 Equipment and Methods 21
   3.2 Comprehensive Experimental Model Analysis 23
      3.2.1 Single Strand 23
      3.2.2 Chamfer 31
      3.2.3 Circular Geometry 37
   3.3 Comparison to Analytic Model 44

4. NUMERICAL MODEL OF 3D PRINTED PART FEATURES 46
   4.1 Model Calibration and Conceptual Model Error 47
   4.2 Verification of Numerical Model 48
      4.2.1 Single String 48
      4.2.2 Chamfer 51
      4.2.3 Circular Geometry 55
   4.3 Comparison to Analytic and Physical Results 59

5. CASE STUDY: DFAM FOR A TOPOLOGY OPTIMIZED COMPONENT 62
   5.1 Design Approach 62
   5.2 Optimizing the Design 62

Page
5.3 Design Analysis 64
5.3.1 Simulation of the Initial Design Approach 65
5.3.2 Applying Design Rules 67
5.3.3 Simulation of the Modified Design Part 68
5.3.4 3D Prints 70
5.4 Results 73
6. SUMMARY, CONCLUSION AND FINAL REMARKS 80
6.1 Summary 80
6.2 Conclusion 83
6.3 Final Remarks 85
LIST OF REFERENCES 88

LIST OF TABLES

Table		Page
3.1	MakerBot parameter setting for printing test specimens	22
3.2	Measured displacement of a single strand at a different temperature	25
3.3	Comparison between the effective modulus computed by the general Equation (Eq. 2.10) and by the modified Timoshenko beam theory (Eq. 2.23)	27
3.4	Comparison of displacement measured and simulated with correction factor $\kappa = 0.94$	28
3.5	Deflection from physical experiment and simulation with various correction factor values of κ	30
3.6	Displacement of one layer strand comparison by measurement and simulation, using Timoshenko's modified beam theory with correction factor $\kappa = 77$.	31
3.7	parameters (protruding length x_0 and displacement y_{max} for prints with different pitch angle α from 15° to 60°	36
3.8	Measurements of prints from merging two geometries with a diameter from 5 mm to 36 mm and an overflow angle $\alpha \approx 30°$	43
4.1	Parameter settings for numerical models for validation of the analytic model and the physical experiments	47
4.2	Parameter setting for numerical model of one single strand at a various temperature	48
4.3	Comparison between the experimental and simulated maximum deflection at the center of the strand.	50
5.1	Comparison between TOD1 and TOD2 (no support) in terms of overall printing time and material usage.	72
5.2	Comparison between TOD1 and TOD2 (with support) in terms of overall printing time and material usage	73
6.1	Design rules for aggregated structures: Overhang-length; pitch angle, Fillets, merged design	83

LIST OF FIGURES

Figure		Page
1.1	Basic elements in general form, from left to right: double-, simple-, non-curved [8].	3
1.2	Topology Optimization on the principle of [11].	4
1.3	From left to right: Geometry in original orientation; efficient orientated; mathematical calculated support structure.	5
1.4	Test specimen for unsupported inner radii r_i [14].	5
1.5	Comparison from the study from Adam and Zimmer [14] and from this research at circular geometry.	6
1.6	CAD models from left to right: pitch-angle of 15° and 45°, circular model and a self-support design layout.	7
2.1	Schematic extrusion process of a FDM printer [24].	10
2.2	Bond formation process (1) layer on layer; (2) bonding process while liquid state; (3) finished bond connection [24].	11
2.3	Fixed supports uniform load deflection model [28].	13
2.4	Comparison of Euler-Bernoulli's (red) and Timoshenko's (blue) beam theory in a overlap [29].	13
2.5	Cantilever beam - single supported and uniform load [28].	14
3.1	MakerBot Replicator 2X, Model 2014, used for all 3D printed parts in this research [31].	21
3.2	Portable digital microscope to measure deflection and surface structure [32].	22
3.3	a) Initial design idea to print one strand and b) realization as a CAD model.	23
3.4	Failed strand print over defined distance L.	24
3.5	Modified (extended support area to the left) design model for one strand prints.	24
3.6	Effective modulus over temperature after calculation of E by the standard displacement equation for cantilever beams - fixed supports on both ends.	26

Figure Page

3.7 Effective modulus over temperature after calculation of E by Timoshenko's modified beam equation (Eq. 2.23). 27

3.8 Error calculation of multiple n-values to compute an effective modulus to correlate to the numerical model. 29

3.9 a) A overview of κ values from initial value to an extreme value to localize the smallest error and b) a detailed view of κ with the smallest error pointed out at $\kappa = 77$. 29

3.10 Effective modulus over temperature by Eq. 2.23. 30

3.11 Illustration of a model definitions as well as the expected print at a 0° overhang print. 31

3.12 Printing failure cause of no support of down-faced parallel areas to the platform at the overhang. As result the tip of each layer drops down. . 32

3.13 Three basic design geometries. (From left: 0° overhang, chamfer and round surface (fillet)). 32

3.14 Overhang print with visualization of pitch angle α at point of bending at each layer. 33

3.15 Two printed overhangs, where the print failed and the layers dropped downwards. It can be noticed that the self-supported layer start dripping at a similar slope. 34

3.16 Print models with a different slope angle α; from left: 15°, 20°, 30°, 45°, 60°. 35

3.17 Illustration of various overhang prints with various pitch angle α. Each print with its measures layer thickness, protruding length and max. displacement (measured in inch - mm values can be found in Table 3.7). The pitch angles are from the top to the bottom as follows: 15°,20°,30°,45°,60°. 37

3.18 Layout of circular geometry on printing platform. 38

3.19 Surface of a printed non-supported round hole. 38

3.20 Print models of round circular geometry with different diameter. 39

3.21 Illustration of the surface after printing round holes without support structure. The bigger r_i gets the more bending at the 0° overhang area appears 40

3.22 Result of Adam et al. [14] research about finding the minimum inner radii for round holes with no need of support at FDM prints. 41

3.23 Design approach for applying minimum α at the overflow from the circle into the tip. 41

Figure Page

3.24 Parts for tests with circular and overhang geometry combined. 42

3.25 Explanation of measured distance of circular height. 42

3.26 Illustration of the surface after printing round holes without support structure. The bigger r_i gets the more bending at the 0° overhang area appears. 44

4.1 Flow chart for the procedure of the numerical model. 46

4.2 Simulation of a single strand at 200°C and $E(T) = 9.53$ GPa. 48

4.3 Simulation of a single strand at 215°C and $E(T) = 3.41$ GPa. 49

4.4 Simulation of a single strand at 225°C and $E(T) = 1.91$ GPa. 49

4.5 Simulation of a single strand at 235°C and $E(T) = 1.30$ GPa. 49

4.6 Simulation of a single strand at 245°C and $E(T) = 1.04$ GPa. 50

4.7 Illustration of printing angle α and layer overhang x_O. 51

4.8 Simulation of $x_O = 0.598$ mm overhang and $\alpha = 15°$. 51

4.9 Simulation of $x_O = 0.405$ mm overhang and $\alpha = 20°$. 52

4.10 Simulation of $x_O = 0.298$ mm overhang and $\alpha = 30°$. 52

4.11 Simulation of $x_O = 0.165$ mm overhang and $\alpha = 45°$. 53

4.12 Simulation of $x_O = 0.006$ mm overhang and $\alpha = 60°$. 53

4.13 Comparison of measured and simulated displacement over overhang angle. 54

4.14 $hole_{diameter} = 5$ mm and a overhang $y_{max} = 0.119$ mm. 55

4.15 $hole_{diameter} = 7$ mm and a overhang $y_{max} = 0.838$ mm. 56

4.16 $hole_{diameter} = 10$ mm and a overhang $y_{max} = 3.17$ mm. 56

4.17 $hole_{diameter} = 20$ mm and a overhang $y_{max} = 4.88$ mm. 57

4.18 $hole_{diameter} = 30$ mm and a overhang $y_{max} = 6.45$ mm. 57

4.19 $hole_{diameter} = 35$ mm and a overhang $y_{max} = 9.31$ mm. 58

4.20 Self-supported design with $hole_{diameter} = 5$ mm, $tip = 0.3$ mm and $y_{max} = 0.36$ mm. 58

4.21 Self-supported design with $hole_{diameter} = 7$ mm, $tip = 0.5$ mm and $y_{max} = 0.29$ mm. 59

4.22 Self-supported design with $hole_{diameter} = 10$ mm, $tip = 0.7$ mm and $y_{max} = 0.26$ mm. 59

Figure Page

4.23 Self-supported design with $hole_{diameter} = 15$ mm, $tip = 1$ mm and $y_{max} = 0.15$ mm. 60

4.24 Simulation of printed self-supported design with $hole_{diameter} = 20$ mm and $tip = 1.3$ mm with a maximum predicted deflection of $y_{max} = 0.12$ mm. 60

4.25 Self-supported design with $hole_{diameter} = 30$ mm, $tip = 1.5$ mm and $y_{max} = 0.1$ mm. 61

5.1 Definition of the design space. 63

5.2 Illustration of both load cases in the case of a chair considered the person is only sitting (top:LC1) and the person not only sitting but also leaning back (bottom:LC2) with both times full support at the bottom. 64

5.3 Initial design approach of a chair printed with 100% support underneath the seating area. 64

5.4 Illustration of the topology optimization process from 100% to final 30% in a low-resolution. The final design will give the best distribution of material withing the design domain to fulfill both load cases. 65

5.5 CAD model of the image from the MATLAB GUI application of the initial topology optimization. 66

5.6 Simulation to predict the deflection of the topology optimized design with low-resolution 67

5.7 Every 0° overhang $\leq$ 0.2 mm (top) becomes a straight line (bottom). Longer overhangs are kept the same. 68

5.8 Design rules applied to the model with changing 0° overhangs ¿ 0.2 mm to a minimum of 25° overhangs as that has been shown as a steady angle for a smooth printing surface. 69

5.9 Design changes from the initial topology optimization design (red outline) with applied design rules (gray model). 70

5.10 CAD model of the modified chair design to avoid 0° overhangs and minimal pitch angle. 71

5.11 Simulation to predict the deflection of the topology optimized design with overhang $\leq$ 0.2 mm changes.$Y_{max} = 0.9$ mm. 72

5.12 Simulation of the second modification with overhang $\leq$ 0.2 mm become a straight line and a chamfer and pitch angle of 25° have been applied. $Y_{max} = 0.12$ mm. 73

5.13 Initial design printed with default settings and full support structure. . 74

Figure Page

5.14 TOD1 printed without any support structure. 75

5.15 Detail view of TOD1 showing the deflection from single layers as predicted in the numerical model. 76

5.16 TOD2 print with default setting for support structure. 77

5.17 TOD2 printed without any support structure. 78

5.18 Detail view of TOD2. 79

6.1 Overview of analyzed aggregated structures with corresponding design rules. From the top: Overhang-length, pitch angle, Holes, merged design 84

6.2 Thermal profile of a 3D printed part at the FDM process.Zone1:heating platform; Zone2: extrusion temperature; Zone3 cooling 86

6.3 Dividing the raft underneath a solid part to take out the thermal stress. 87

ABSTRACT

Lischke, Fabian. M.S.M.E., Purdue University, May 2016. Design of Self-supported 3D Printed Parts for Fused Deposition Modeling. Major Professor: Andrés Tovar.

One of the primary challenges faced in Additive Manufacturing (AM) is reducing the overall cost and printing time. A critical factor in cost and time reduction is post-processing of 3D printed (3DP) parts, which includes removing support structures. Support is needed to prevent the collapse of the part or certain areas under its own weight during the 3D printing process.

Currently, the design of self-supported 3DP parts follows experimental trials. A trial and error process is needed to produce high quality parts by Fused Depositing Modeling (FDM). An example for a chamfer angle, is the common use of 45° angle in the AM process. Surfaces that are more flat show defects than inclined surfaces, and therefore a numerical model is needed. The model can predict the problematic areas at a print, reducing the experimental prints and providing a higher number of usable parts.

Physical-based models have not been established due to the generally unknown properties of the material during the AM process. With simulations it is possible to simulate the part at different temperatures with a variety of other parameters that have influence on the behavior of the model.

In this research, analytic calculations and physical tests are carried out to determine the material properties of the thermoplastic polymer Acrylonitrile - Butadiene - Styrene (ABS) for FDM at the time of extrusion. This means that the ABS is going to be extruded at 200°C to 245°C and is a viscus material during part construction.

Using the results from the physical and analytical models, i.e., Timoshenko's modified beam theory for micro structures, a numerical material model is established to simulate the filament deformation once it is deposited onto the part. Experiments were also used to find the threshold for different geometric specifications, which could then be applied to the numerical model to improve the accuracy of the simulation.

The result of the nonlinear finite element analysis is compared to experiments to show the correlation between the prediction of deflection in simulation and the actual deflection measured in physical experiments.

A case study was conducted using an application that optimizes topology of complex geometries. After modeling and simulating the optimized part, areas of defect and errors were determined in the simulation, then verified and and measured with actual 3D prints.

1. INTRODUCTION

1.1 Motivation

Numerical models are very rare in the area of simulating Fused Deposition Modeling (FDM) 3D prints at the point of extrusion. Simulations depend on unknown material properties at the time of extrusion.

Support material waste is a significant issue in additive manufacturing. Support material is necessary in additive manufacturing when a particular geometry has no material underneath it in relation to the print platform. Case studies show that support material waste is reduced up to 40% by using Additive Manufacturing (AM) instead of Subtractive Manufacturing (SM) [1] processes. The development of more robust methodologies for designing AM processes can save almost half of the raw support material compared to SM, and is therefore a topic worthy of further examination. This research focuses on part design modification in order to create self-supported 3D printed parts. The goal is to develop self-supporting geometries so that FDM support material may be omitted. This will not only help to reduce support material but also will have an impact on lowering the overall printing time and manufacturing costs of a part. By modifying the part design, time is no longer wasted removing support material.

Many studies have been part design optimization, few focus on optimizing the support structure by re-positioning the part [2,3]. Fewer studies consider re-designing the part for self-supported features. Another under-explored topic are the material characteristics at the time of printing and the way in which these characteristics contribute to the integrity of the final print. Material properties for ABS in its solid state are well known, but ABS at time of extruding, where its behavior is viscus is relatively unknown. However, ABS behavior in a viscous state at the time of extruding

is relatively unknown. In the study from Naghieh et al. [4] finite element analysis was used to develop a numerical model to assess the effects of layer penetration on inter-layer adhesion, which is reflected on the mechanical properties of bone scaffolds. However, their study determines the material properties after printing the model and not during the time of extrusion. This research will therefore center on both the redesign of parts to reduce support structure and the analysis of material properties and behavior at the point of filament extrusion.

1.2 State of the Art in Design for Additive Manufacturing

New methods and rules for designing a part have to be considered to benefit from the potential from AM [5]. In 1958 Design for Manufacturing (DfM) for metal parts was introduced by W. Bolz in his book "Metals Engineering Processes" [6]. In short, the primary objective of DfM is to eliminate manufacturing difficulties and reduce costs [7]. Once AM began to permeate the discourse of mainstream manufacturing, it became necessary to redefine DfM. D. Rosen (2007) coined the term Design for Additive Manufacturing (DfAM) to describe [7]:

"Synthesis of shapes, sizes, geometric meso-structures, structures between 0.1 and 10 mm, material compositions and micro-structures, structures < 0.1 *mm [5], to best utilize manufacturing process capabilities to achieve desired performance and other life-cycle objectives."*

The development and research of DfAM has increased and researchers began to explore different design rules for additive manufacturing processes. G. Adam and D. Zimmer have studied three different AM processes, Laser Sintering (LS), Laser Melting (LM) and FDM. In their research they investigated multiple designs with the same boundary conditions but different manufacturing processes [8]. The focus of their research was on three general forms of basic elements (Figure 1.1), double curved, simple curved, and non-curved [8].

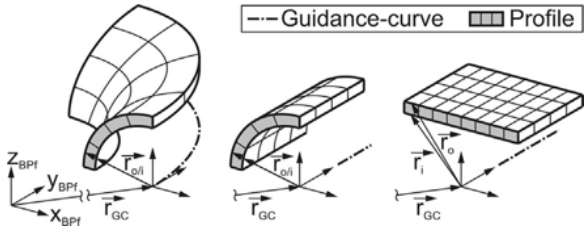

Figure 1.1 Basic elements in general form, from left to right: double-, simple-, non-curved [8].

Adam and Zimmer [8] analyzed these basic element forms according to a set of rules which were developed to measure the success of each form according to both its final outcome and the feasibility of the print operation. The design rules they invented can be applied to geometries such as edges, gaps, overhangs and islands of 3D printed parts. 2012 Vayre et al. [9] studied a methodology that follows fours steps of designing parts for AM. Step one analyzes the specifications of the part. The next step initiates the shape. The third step defines and optimizes parameters of the design. The final step validates the manufacturability of the optimized shape. This procedure is well known and is used in many studies about DfAM. A global approach for DFAM has been developed for the functional specifications and the process characteristics by Ponche et al. [10]. Many research papers address the topic of DfAM in an overall process, but only few consider the improvement of design parts such as manufacturability [10].

Since there are many different processes of AM, it is first necessary to summarize the current knowledge of DfAM at FDM. The process of support material reduction forms the basis of this study. There are multiple ways to reduce the support material. One way is to adopt the methodology of Topology Optimization (TO). Another way is adapting the knowledge of Topology Optimization (TO) not at the design part itself but at the support structure [11]. In this methodology, the total print object is divided into two pieces: the design space (actual part) and non-design space (support material), illustrated in Figure 1.2.

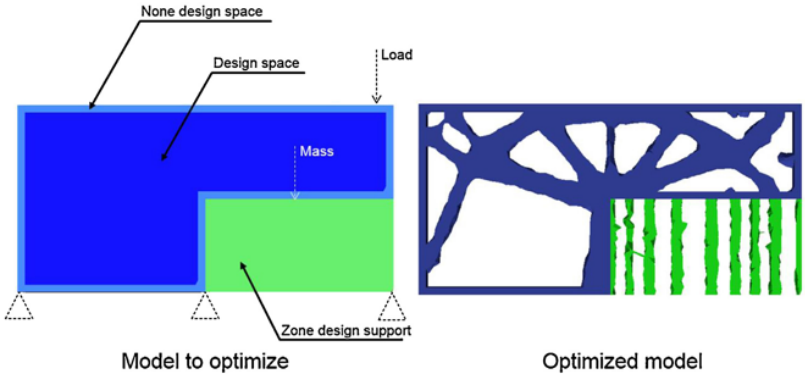

Figure 1.2 Topology Optimization on the principle of [11].

This allows the non-design space to be treated separately, so that the volume of material can be optimized [11], using the methodology of TO. Another approach to reduce support material at 3D Printing (3DP) involves the strategic placement of the model [3]. In the study of Strano et al. [2] optimization of the support structure is based on mathematical algorithms. After placing the design part in the most efficient way in the printing software, model data can be imported into MATLAB for further analysis. An algorithm, based on implicit functions, will compute and create a micro-structure support and specified volume fractions [2]. By adding the term k to a trigonometric function

$$cos(k_x x) + cos(k_y y) + cos(k_z z) = 0, \tag{1.1}$$

it is possible to change the periodicity of the trigonometric term as well the cell periodicity, which is needed for different cellular structures of the support design. Figure 1.3 displays the approach [2] with first placing the design in a position where minimum support is needed and after that, the micro-structure support developed by an algorithm.

Another approach for changing the support structure is to apply the methodology of cellular structure to the support instead the model itself. D. Rosen and P. Chang discuss the topic in their journal of a synthesis method for the design of meso-scale

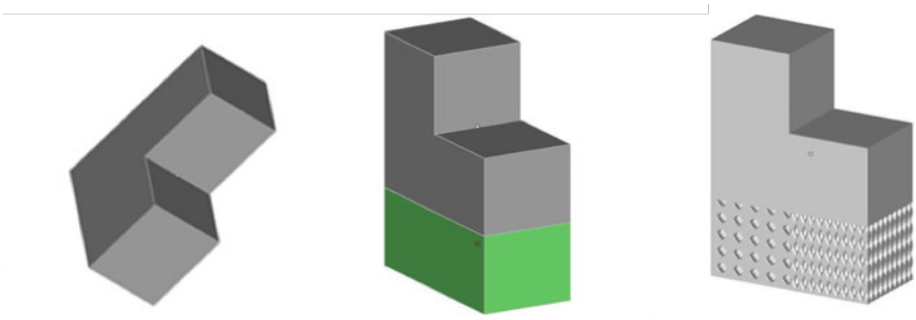

Figure 1.3 From left to right: Geometry in original orientation; efficient orientated; mathematical calculated support structure.

cellular-structures [12]. In the research they show a conversion from a solid-body to a topology optimized cellular-body. The cellular optimization is a different method of topology optimization as compared to the "spider-web" optimization [11, 13].

Adam et al. [14] studied the manufacturability of test specimens with down-facing surfaces (Figure 1.4) for FDM. They studied bore designs to find out the suitable inner radii r_i without use of support material [14].

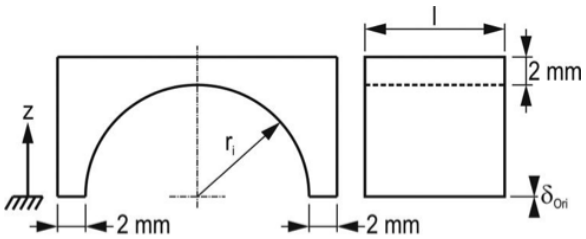

Figure 1.4 Test specimen for unsupported inner radii r_i [14].

Their work showed that for FDM prints an acceptable inner radius of $r_i \leq 5$ mm is manufacturable. $R_i > 5$ mm resulted in defected or even destroyed surfaces (Figure 1.5).

Adam et al. [8] did not consider the overhang-to-radii ratio which can increase the value of the inner radii for manufacturability. They defined the suitable overhang for FDM prints at $l_{Overhang} = 1.8$ mm. Everything greater than that will collapse because a self-support of each layer is not possible [8]. Thomas [15] covers the printing angle

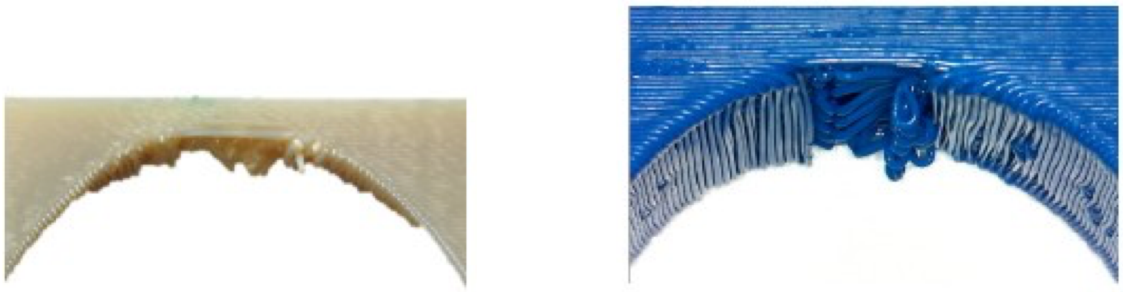

(a) print output from Adam and Zimmer [14]

(b) print output from research

Figure 1.5 Comparison from the study from Adam and Zimmer [14] and from this research at circular geometry.

of Selective Laser Melting (SLM) of 45° and others with minimum of 38° [16] and a minimum of 20° [17]. Results found for SLM where adapted to the FDM process. Currently printing companies like MakerBot, as well as model-slicing software such as Slic3r, use 45° as a default setting [18]. A design approach for printing self-supporting structures using FDM has not been fully addressed.

1.3 Research Gap in Simulation-based Design for Additive Manufacturing

There is a lack of research addressing a comprehensive solution which integrates AM capabilities as well as limitations of AM into a topology optimization algorithm (D. Rosen [13]). Next to topology optimization, issues of integrating AM building processes in a numerical model can hardly be found in literature for the FDM process, one AM numercial model which is been used by companies to determine damage and critical areas at the print is GENOA from AlphaSTAR Corporation [19]. Most of the prior research on minimizing the support structures are focusing on re-positioning the model or defining a different approach to recalculate the support. A numerical model would fill the gap and reduce the prints of trial and error, where parts show defects due to improper supported or over supported areas. To simulate the prints

at extrusion time, the material properties have to first be defined. The knowledge of an analytic model that is capable of determining material properties (such like a effective modulus of ABS at printing time) has to be developed, since it can not be found in any literature. This thesis aims to provide a basis for when and how to apply certain design features, based on well established design rules [8, 14] while also developing new design rules. The research covers an unknown area of implementing rules into a numerical model to predict any defects in the model. Also it collaborates with the methodology of topology optimization, so that both part material as well as support material will be minimized simultaneously in one procedure.

1.4 Objective

The objective in this research is to develop a preliminary design approach of self-supported structures using FDM AM processes. Instead of optimizing the support structure of the print, design rules will be developed to address design modification. These modifications will decrease the amount of support material required for a particular print. The main focus lies on ABS material parameters at the time of filament extrusion through a analytical model of a modified Timoshenko beam theory. This will then be implemented into a finite element analysis (FEA) software. By measuring deflection from single or multiple layers (found through multiple physical experiments) a numerical model may be validated and fully realized. This approach has been implemented for structures with different geometric forms, such as a variety of pitch angles from 15° to 60° or more complex circular models (Figure 1.6) and loading conditions.

Figure 1.6 CAD models from left to right: pitch-angle of 15° and 45°, circular model and a self-support design layout.

The analytic results were established, based on Timoshenko's beam theory. The model, developed in Wang et al. [20], has been modified and adapted to the conditions used in this approach. In order to ensure the benefit and usability of the design approach, a case study has been presented in this research. The simulation model combined with the topology optimization model from Tovar and Liu [21] has been used to minimize the support and make it producible by applying the design approach developed in this work.

1.5 Research Approach

This thesis is constructed in the following manner: Chapter 1 presents a literature review of design for AM and gives an overview of what the research can change in the area of FDM 3D printing. The analytic model based on Timoshenko's beam theory is explained and compared to Euler–Bernoulli's beam theory in Chapter 2 with a summary of results. In Chapter 3 the physical experiments are described as well as a comparison to the previous developed analytic model. The results found in Chapter 2 and 3 are implemented in a numerical model in ANSYS in Chapter 4. With help of the developed material properties and the simulation model, a prediction of behavior for a printed part can be obtained. This is demonstrated in Chapter 5 by a case study, where support structure is being optimized and conserved with help of the analytic and numerical model. The last chapter (Chapter 6) will summarize the results as they have been developed throughout this work as well as future recommendations associated with this research.

2. ANALYTIC MODEL OF EXTRUDED FILAMENT

2.1 Fused Deposition Modeling Process

Fused Deposition Modeling (FDM) is an additive process to manufacture thermoplastic parts. Those parts are created through a melted thermoplastic strand of ABS or Polylactic acid (PLA), by bonding multiple layers on top of each other. Since 1989, Stratasys Ltd. has a patent on the FDM process [22]. This process was introduced the first time in the USA in 1991 and in Europe three years later. Since 2003 FDM has been the most prolific additive manufacturing process to manufacture prototypes as well as smaller series productions. The following will address the FDM process for a better understanding in context with this research. As references D. Rosen, I. Gibson and B. Stuckers book about Additive Manufacturing Technologies [23] as well as other publications [24–26] have been used. Features that need to be addressed are:

- Extrusion of the material through the heated nozzle
- Bonding printing material to support structure
- Bonding of the material to itself
- Support structure for a wide range of geometrical designs

One important process in FDM that effects all the following steps is liquefying the thermoplastic material in the heated nozzle. The material, ABS or PLA will be unloaded from the spools and extruded through the nozzle, T_{nozzle} at about 220°. To realize the print, a slicing software takes the STL-File and divides the computer model into layers to develop a compatible path for the material to be extruded. Following that, the software generates and sends the commands to the printer. The printer will execute the code for a layer-by-layer printed solid model, illustrated in Figure 2.1.

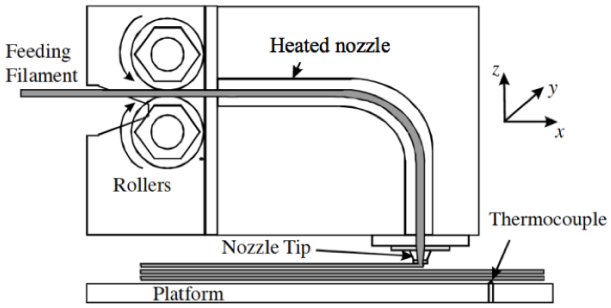

Figure 2.1 Schematic extrusion process of a FDM printer [24].

For a high resolution print, two parameters have to be covered that have an effect on the outcome. Extrusion speed through the printing head depends on temperature as well as feed velocity. The correct ratio between temperature and feed velocity will lead to superior resolution of the model. If the temperature is too high, material will get burned inside the head. Also it needs longer to cool down after extrusion. If it is too cold, the material may clog the head and not extrude. Also the next layer will not bond correctly with adjacent material on the platform [23]. The feed velocity needs to be controlled to provide a constant volumetric flow rate of material, Q. The linear feed velocity, v_{feed}, of the filament through the nozzle can be approximated as follows [25]:

$$v_{feed} = \frac{Q}{WH}. \tag{2.1}$$

Here W stands for a desired road width and H the slice thickness. After extrusion of the material, each layer has to connect to the previous one on the platform. Besides material properties, the bonding process is also defined by temperature either in the chamber, if it is an enclosed system, or the environmental temperature, in an open systems. The bonding will determine if the part has some structural defects or an overflow in one of its layer. In 1996 Yardimci and Güçeri defined a bonding potential ϕ with an integral over time t, with a critical temperature T_c, interface Temperature T and an integration variable $d\tau$ [26]:

$$\phi = \int_0^t (T - T_c) d\tau \tag{2.2}$$

The bonding potential will help to determine how the bond process finishes. The higher the bonding potential ϕ is, the stronger the bond between each layer will occur. Using a different material for support, will effect the bonding. The material properties of support material differ from the ones of the printing material (ABS or PLA). The support material needs to be removed after the model is printed and can not be bonded with the final model as with the same strength as the layers printed with the same FDM material. Removing support structure can be achieved by placing the part in a tank with a water-mixture that dissolves the support material or breaks it away. Nonetheless the materials need to be connected to each other in a way that it will offer support for the final model during the print but also leave no physical trace on the printed object after it has been removed. With a design approach for self-supported structures the issue of removing support in post-processing can be ignored. Figure 2.2 illustrates the bonding formation process, which shows the link between model material and support material.

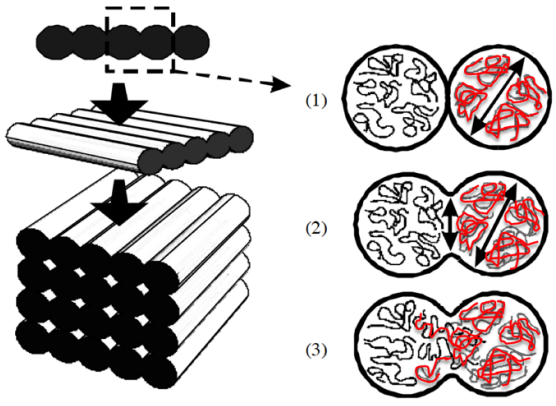

Figure 2.2 Bond formation process (1) layer on layer; (2) bonding process while liquid state; (3) finished bond connection [24].

As a recap of the above explained variables it can be said that while printing with FDM. It is important to have a steady design while printing with FDM. Parameters like bonding or feed velocity will interact with the design and enable a more complex design geometry previously not possible.

2.2 Design Formulation

In general, a beam deformation problem is known as a Euler-Bernoulli (EB) beam theory. This theory is defined through cross-sections in unloaded conditions at a right angle to the zero line that are aligned, and remain planar even in deformation. For the extended beam theory this will not be accepted, where in addition to EB a cross-sectional plane rotates about a thrust angle. This beam theory is known as the Timoshenko beam (Tb) theory. The Tb theory takes into account that the shear deformation of the cross-sectional plane is nonzero [27]. The following section covers a method to analyze a cantilever beam with length L, fixed supports and uniform load w as shown in Figure 2.3. Multiple elements for a linear static deflection of a cantilever composite beam subjected to a uniform load and temperature are studied for both EB and Tb theory. However, for simplification of the problem and as a foundation for the numerical model, the objective was not to simulate the printing process layer-by-layer, but rather the main deflection and prediction of critical areas of the part itself after printing. Therefor a linear deflection was used. In a numerical model where each layer will be simulated, a non-linear solution needs to be considered because of the behavior of ABS at high temperatures, as well as a dynamic modulus with a viscoelasticity E^*. In the following section, the goal was to compute the effective modulus of ABS at different temperatures with a simplified linear model. The computation was performed in term of the Young's modulus but was re-named as the effective modulus, since the material properties do not satisfy the requirements for the definition of a Young's modulus. Nonetheless, in the numerical model it has to be substituted for the Young's modulus to avoid confusion.

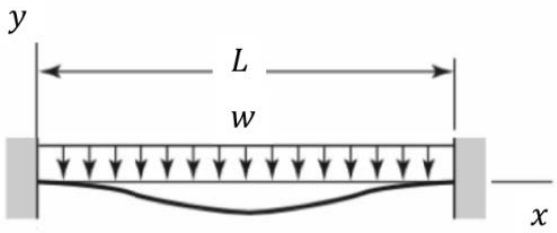

Figure 2.3 Fixed supports uniform load deflection model [28].

For a large length-diameter-ratio at beams, displacement y_{max} due to shear becomes important, which is included into of the formulation of Tb theory [20]. Figure 2.4 displays the visual difference between the EB beam and Tb theory.

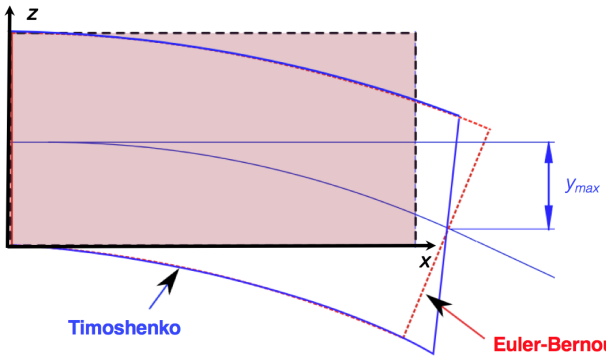

Figure 2.4 Comparison of Euler-Bernoulli's (red) and Timoshenko's (blue) beam theory in a overlap [29].

The next two sub-sections will derive the EB as well as the Tb theory and point out the necessity to use the Tb theory. By modifying Wangs et al. [20] developed Tb theory for micro scaled beams, it is possible to analyze the deformation of micro diameter layer 3D printed models. This solution will allow for printed parts, to re-design support structure dependent on the result and also to develop a numerical model, which is discussed in Chapter 4.

2.2.1 Euler-Bernoulli Beam Theory

Bernoulli's assumptions are named after Jacob Bernoullis (1750) simplifications of the linear theory of elasticity for load carrying beams. The relevant assumptions are following:

- length of the beam greater than the cross-section
- the center of mass at the cross-section is subject to only one shift
- no warping
- small deformation
- 1-D stress state

The formulation below defines the analytic way of computing deformation with the EB beam theory, a single supported beam (Figure 2.5) with respect to the work of Zindler and his work about varying beam theories and the deformation as a central element [30]

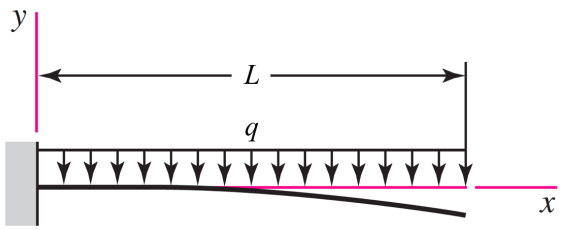

Figure 2.5 Cantilever beam - single supported and uniform load [28].

Initial Eq. 2.3 for EB is given as follows:

$$EIy^{IV} - q = 0, \tag{2.3}$$

where q is the uniformed load and for further computation it is considered as the dead load of the beam. Under a uniform load the EB beam function becomes a 4^{th} order polynomial. E represents the effective modulus and I the moment of inertia at the specific shape. After the next three derivations:

$$\dddot{y}_{EB} = \frac{q}{EI} \int dx, \tag{2.4}$$

$$\ddot{y}_{EB} = \frac{q}{EI} \int \int dx = \frac{q}{EI} \int (x + C_1) dx = \frac{q}{E}(\frac{1}{2}x^2 + C_1 x + C_2), \tag{2.5}$$

with x as the point of deflection and integration constants C_1 and C_2 as boundary conditions

$$y_{EB} = L \rightarrow C_1 = -\tfrac{1}{2}L,$$

and

$$y_{EB} = 0 \rightarrow C_2 = 0$$

the first derivation becomes:

$$\ddot{y}_{EB} = \frac{q}{2EI} \int (x^2 - xL) \cdot dx. \tag{2.6}$$

The deflection y_{EB} with two additional integration constants C_3 and C_4 becomes:

$$y_{EB} = \frac{q}{2EI}(\frac{1}{12}x^4 - \frac{1}{6}x^3 L + C_3 x + C_4) \tag{2.7}$$

for

$$y_{EB} = L \rightarrow C_3 = \tfrac{1}{12}L^3,$$

and

$$y_{EB} = 0 \rightarrow C_4 = 0.$$

The final equation for deflection at the EB theory will become:

$$y_{EB} = \frac{qL^4}{24EI}(\frac{x^4}{L^4} - 2\frac{x^3}{L^3} + \frac{x}{L}). \tag{2.8}$$

In terms of maximum deflection with $x = \frac{L}{2}$ and bending in negative y-direction, Eq. 2.8 becomes the most common used formula

$$y_{EB-max} = -\frac{5qL^4}{384EI}, \tag{2.9}$$

and in terms of effective modulus E it can be re-written as

$$E = -\frac{5qL^4}{384y_{EB-max}I}. \tag{2.10}$$

2.2.2 Timoshenko's Modified Beam Theory

Timoshenko's beam (Tb) theory is an extension of the classical beam theory after EB. Additional to EB, the effect of shear deformation is considered in Tb calculations for deformation as well as one additional assumption to the already known effects from EB is required.

- The normal to the cross-section is not necessary parallel to the tangent of the deformation

With this additional assumption Tb can be written as it is derived and established in [30] (Eq. 2.11):

$$y_{Tb} = y_{EB} - \int \frac{Q(x)}{\kappa GA} dx \tag{2.11}$$

Here κ is a correction factor that is based on the Poisson's ratio, G shear modulus and A area of the cross-section. $Q(x)$ is a function of the load, which acts on the

beam and will become zero if shear deformation is considered. With $Q(x) \propto -\int q dx$ Eq. 2.11 can be re-written as:

$$y_{Tb} = y_{EB} + \frac{1}{\kappa GA} \int \int q(dx)^2. \tag{2.12}$$

After considering boundary conditions for x and substituting it in both integration constants C_1 and C_2 as follows:

$$x = L \rightarrow C_1 = -\tfrac{L}{2},$$

and

$$x = 0 \rightarrow C_2 = 0,$$

the final Tb equation for deflection at a single supported beam becomes:

$$y_{Tb} = y_{EB} + \frac{2}{2\kappa GA}(x - L). \tag{2.13}$$

Eq. 2.13 is the general used form for a beam problem computed with Timoshenko's approach considering shear deformation.

This research required a method able to predict and compute the deformation of single or multiple ABS printed layers. In the work of Wang et al. [20], a micro scale Tb model has been developed, based on strain gradient elasticity theory. This model can be applied to the classic Tb model when relevant parameters are being changed or set equal to zero. The approach from Wang et al. [20] appeared to be a more accurate fit to the problem addressed in this research than the EB beam theory. Since the thermoplastic material behavior at point of extrusion is viscous and cannot be considered solid, a variance of the general form of Timoshenko had to be implemented. In order to develop the deflection at the beam at any given point x following Fourier series derived by Wang et al. [20]:

$$y(x) = \sum_{n=1}^{\infty} W_n sin(\frac{n\pi x}{L}). \tag{2.14}$$

In Eq. 2.14 W_n is a Fourier coefficient that needs to be calculated for each n. In this research $n = 1$. Furthermore governing equations for the static problem need to be defined as [20] gives them by:

$$\begin{aligned} q &= (k_3 + k_4)y^{IV} + (k_3 - 2k_4)\dddot{\psi} - k_5(\ddot{y} - \dot{\psi}). \\ 0 &= k_1\psi^{IV} - (k_3 - 2k_4)\dddot{y} - (k_2 + k_3 + 4k_4)\ddot{\psi} - k_5(\dot{y} - \psi). \end{aligned} \tag{2.15}$$

The terms of k_n with $n = 1, 2, 3, 4, 5$ represent model parameters, load and reference length of the beam. ψ defines rotation of line elements along the center line due to bending [20]. The applied load $q(x)$ given in a Fourier series is established as:

$$q(x) = Qsin(\frac{\pi x}{L}). \tag{2.16}$$

Wang et al. [20] defines the in Eq. 2.16 mentioned applied load like follows:

$$Q = \frac{2P}{L}sin(\frac{\pi}{L}). \tag{2.17}$$

In this research two material length scale parameters (l_1 and l_2) are set to zero and therefore k_3 and k_4 are zero. This will lead to the modified model used in the computation for the effective modulus. All k_n variables are defined as:

$$\begin{aligned} k_1 &= I(2\mu l_0^2 + \frac{4}{5}\mu l_1^2) \rightarrow l_1 = 0 \rightarrow k_1 = I2\mu l_0^2, \\ k_2 &= I(K + \frac{4}{3}\mu) + 2\mu A l_0^2, \\ k_3 &= \frac{1}{4}\mu A l_2^2 \rightarrow l_2 = 0 \rightarrow k_3 = 0, \\ k_4 &= \frac{8}{15}\mu A l_1^2 \rightarrow l_1 = 0 \rightarrow k_4 = 0, \\ k_5 &= \kappa\mu A, \end{aligned} \tag{2.18}$$

where K represents the bulk modulus, μ the shear modulus, l_0 is the material length scale parameter and κ the correction factor. For a cylindrical geometry, used in this research, the moment of inertia I is given by

$$I = \frac{\pi d^4}{64}, \tag{2.19}$$

with d as the diameter of the printed thermoplastic. As far as the - to be defined - variable of the effective modulus E, the bulk and shear modulus need to be written in terms of E and Poisson's ratio ν as

$$\begin{aligned} K &= \frac{E}{3(1-2\nu)} \\ \mu &= \frac{E}{2(1+\nu)} \end{aligned} \tag{2.20}$$

After every variable and equation has been defined and simplified, W can be determined by substituting Eq. 2.14, 2.16 and 2.17 in Eq. 2.15 as

$$W = \frac{\alpha^4 k_1 + \alpha^2 k_2 + k_5}{\alpha^2 k_5[\alpha^4 k_1 + \alpha^2 k_2 + k_5] - [\alpha k_5]^2} \frac{2P}{L} sin(\frac{\pi x}{L}), \tag{2.21}$$

where $\alpha = \pi L$ represents a geometric parameter and x the point of deflection. For the maximum deflection $x = \frac{L}{2}$. With that condition and in terms of E, the maximum deflection of a micro scaled Timoshenko beam based on the strain gradient elasticity theory and the work of [20] can be written as follows:

$$\begin{aligned} y_{max} = &\frac{2P(2\nu-1)(\nu+1)^2}{EALk_s\alpha^2(2\nu^2+\nu-1)} \\ &\frac{(Ak_s - 2A\nu + 2I\alpha^2 + 2A\alpha^2 l_0^2 + 2I\alpha^2 l_0^2 - 2I\alpha^2\nu^2 - 4A\alpha^2 l_0^2\nu - 4I\alpha^2 l_0^2\nu)}{(Ak_s - 2Ak_s\nu + I\alpha^2 + A\alpha^2 l_0^2 + I\alpha^2 l_0^2 - I\alpha^2\nu^2 - 2A\alpha^2 l_0^2\nu - 2I\alpha^2 l_0^2\nu)}, \end{aligned} \tag{2.22}$$

transposing Eq. 2.22 after effective modulus E it becomes:

$$E = \frac{2P(2\nu-1)(\nu+1)^2}{y_{max}ALk_s\alpha^2(2\nu^2+\nu-1)} \frac{(Ak_s - 2A\nu + 2I\alpha^2 + 2A\alpha^2 l_0^2 + 2I\alpha^2 l_0^2 - 2I\alpha^2\nu^2 - 4A\alpha^2 l_0^2\nu - 4I\alpha^2 l_0^2\nu)}{(Ak_s - 2Ak_s\nu + I\alpha^2 + A\alpha^2 l_0^2 + I\alpha^2 l_0^2 - I\alpha^2\nu^2 - 2A\alpha^2 l_0^2\nu - 2I\alpha^2 l_0^2\nu)}. \quad (2.23)$$

2.3 Summary

The developed equations for FDM models used in this research are based on a theory, which considers shear from Thimoshenko's beam theory. Modifications were necessary to apply Timoshenko's beam theory, as it already was modified by Wang et al. [20] for utilizing design features. The standard general deflection equation from Euler-Bernoulli's theory is not applicable. With regard to a large length-diameter ratio, Timoshenko's equation can be applied for computing the effective modulus E. The effective modulus represents the Young's modulus to correlate to the numerical model as explained in Chapter 4. After considering the boundary as well as the initial conditions, the results from this chapter can be implemented in a finite element analysis software to predict the behavior of 3D-printed FDM parts.

3. PHYSICAL TESTING

3.1 Equipment and Methods

The first prints for this research, sub-section Single strand, where printed on a commercially available assembly kit which cost around $800 USD. The print results of these early experiments were inconsistent in quality and structural integrity, so further experiments were performed with a MakerBot Replicator 2X, Model 2014 (Figure 3.1)

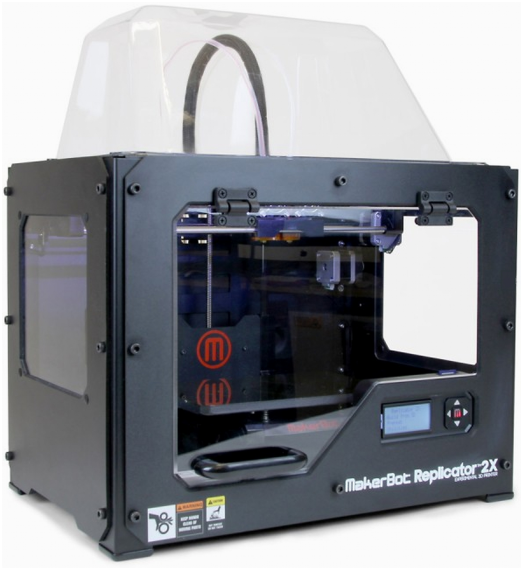

Figure 3.1 MakerBot Replicator 2X, Model 2014, used for all 3D printed parts in this research [31].

Default settings were used to control all features except for the nozzle, which was changed to a 0.3 mm diameter printing nozzle and the temperature $T_{extrusion}$, which was variable. All parameters and how they have been used are listed in Table 3.1.

Table 3.1 MakerBot parameter setting for printing test specimens

Extrusion temperature [°C]	225
Extrusion speed $[\frac{mm}{s}]$	40
Platform temperature [°C]	115
Number of shells	3
Layer height [mm]	0.3
Infill density [%]	10
Infill pattern	diamond
Active chamber heating control	no

The visual measurements have been carried out with a digital microscope (Figure 3.2). The images where taken with a 250x magnification at a 1600x1200 px snapshot setting.

Figure 3.2 Portable digital microscope to measure deflection and surface structure [32].

For verification between the analytical model and physical experiments, all calculations had been carried out in MATLAB. To verify and compare the results, measured at the 3D prints, the physical and the numerical models, have been simulated, described in Chapter 4, in a finite element analysis software, ANSYS 16.2. The mod-els have been implemented from PTC Creo Parametric, a Design-CAD software, or designed and taken directly over from ANSYS Workbench, Modeling sub program to ANSYS Structural Analysis.

3.2 Comprehensive Experimental Model Analysis

The up coming sections demonstrate and delineate the different experiments that have been accomplished within this research. The physical experiments are carried out to develop material properties of ABS as well as helped to adjust the numerical model.

3.2.1 Single Strand

The purpose of printing one single strand will help to determine multiple parameters at FDM printing that have not been explored before. The design idea of just printing one strand is based on the fixed support beam model (Figure 3.3a). The printer prints a support area in a defined distance and a single strand on top, like the CAD model also illustrated in Figure 3.3b

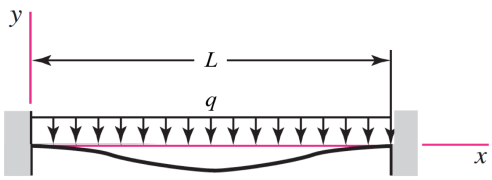

(a) Fixed supported beam - uniform load [28].

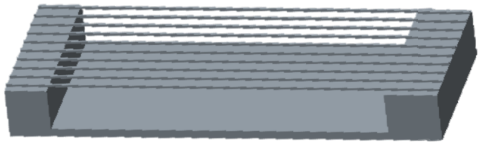

(b) CAD model.

Figure 3.3 a) Initial design idea to print one strand and b) realization as a CAD model.

With this design, different parameters and variables that have an effect on the print cannot only be calculated, simulated and verified with physical experiments. The uniform load over the beam or with the printed strand is the dead load. In the case of the strand, it is calculated by the density of the material as well as the area and gravity. The one variable which needs to be determined. Indeed, the main purpose of this experiment is to determine the effective modulus E at a different temperature. For the thermoplastic ABS, E is known and written down in a range

from 1.7 GPa to 2.8 GPa. This is at a solid state of ABS. As mentioned before at extrusion, ABS is viscous behavior and therefore E is not specific enough for an accurate prediction in simulations of printed parts. With the one strand model, E can be measured and calculated for verification by the earlier derived modified Timoshenko beam theory for micro-scale beams (Eq. 2.23). This leads to a effective modulus temperature dependence and constant extrusion velocity. The results shown in the next sub section will be used for the numerical model to predict deflection, which is addressed in Chapter 4.

One-Strand Experimental Results

First prints of the design need to be adjusted because of failure during the print. The strand was not extruded properly and it was not able to print a constant solid strand over a defined distance L, shown in Figure 3.4.

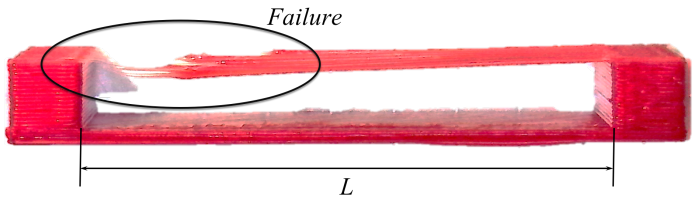

Figure 3.4 Failed strand print over defined distance L.

The necessary design change for this experiment, which was made for this experiment, was to extend the support area where the printer starts to print the strand so that the material can be extruded in a sufficient way and time, compare Figure 3.5.

Figure 3.5 Modified (extended support area to the left) design model for one strand prints.

For this research five different models at five different temperatures have been printed. The temperature of default extruded thermoplastic ABS is from 220° to 230°. For research purposes the temperature was lowered to a minimum of 200° and increased to a maximum of 245° to determine the maximal bending at $\frac{L}{2}$ of one strand. The results of the maximum deflection at each model is listed and illustrated in the following Table 3.2.

Table 3.2 Measured displacement of a single strand at a different temperature

Temperature [°C]	Displacement y_{max} [μm]	Single strand test print
200	64	
215	179	
225	319	
235	469	
245	589	

It clearly can be seen that the displacement increases enormously with temperature increase. This can be explained physically because of the viscosity of ABS: at higher temperature it needs more time to cool down after extrusion. With those measurements of the physical experiments, a graph for a temperature dependent effective modulus can be established for the time of extrusion at a FDM printer, see Figure 3.6 below.

E was computed by the general deflection for cantilever beams with fixed supports on both ends. Eq. 2.10 is the standard equation for a beam fixed on one end. The equation that has been used here is

$$E = -\frac{qL^4}{384 y_{max} I}. \tag{3.1}$$

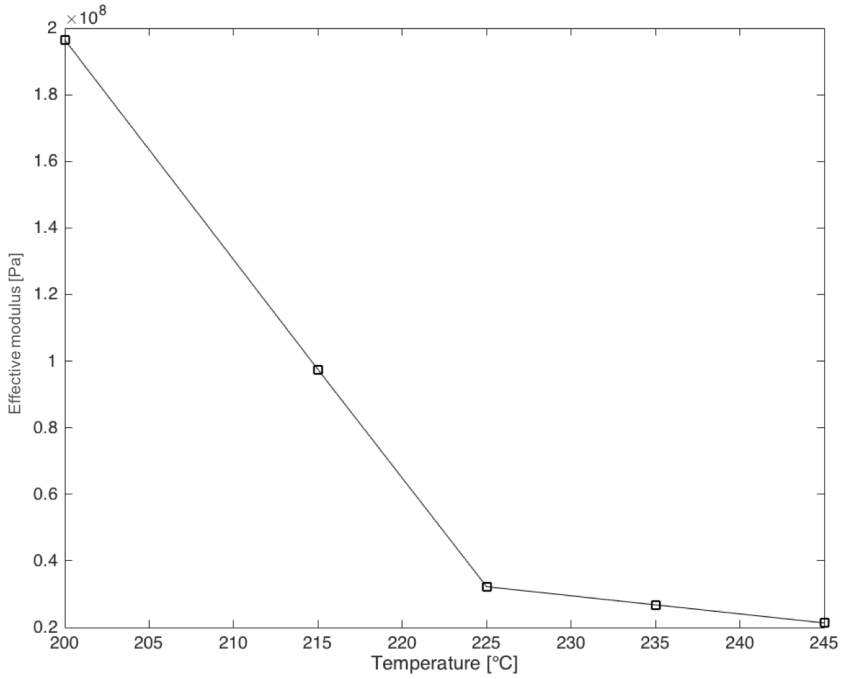

Figure 3.6 Effective modulus over temperature after calculation of E by the stan-dard displacement equation for cantilever beams - fixed supports on both ends.

For this research the method from Timoshenko has been modified, E was also computed with the developed equation in Chapter 2 (Eq. 2.23). In Timoshenko's theory another important constant had to be defined, which is the shear coefficient. Many authors developed through different approaches the most accurate coefficient and came up with a definition for the correction factor κ. The first calculations had been executed with

$$\kappa = \frac{6 + 12\nu + 6\nu^2}{7 + 12\nu + 4\nu^2}, \tag{3.2}$$

as this is titled the best expression for cylindrical cross-section beams by T. Kaneko [33]. As before, both ends of the strand are fixed support for the κ which departs from the value found in [33]. By using Kaneko's definition and the modified Eq. 2.23 following E (Figure 3.7) could be computed for this experiment.

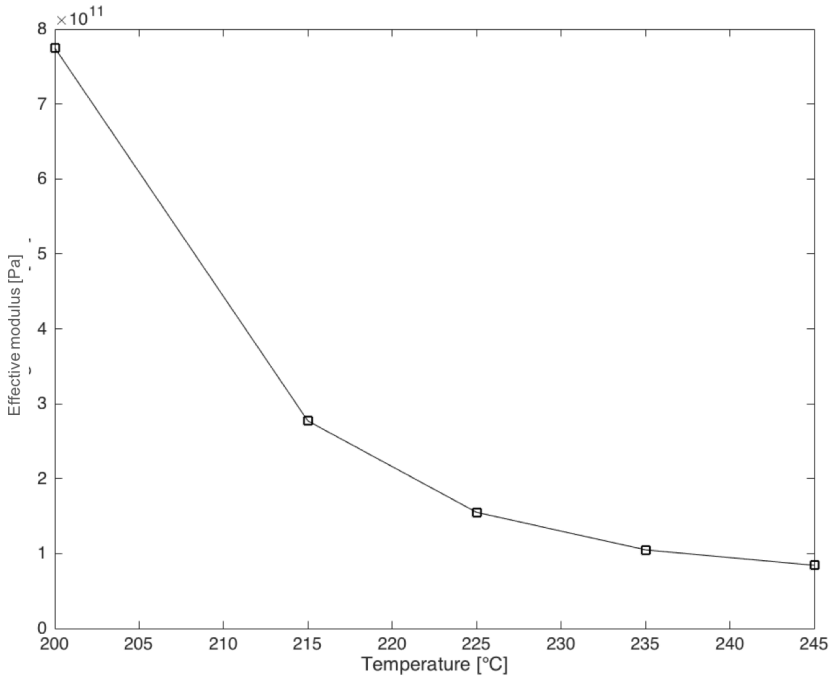

Figure 3.7 Effective modulus over temperature after calculation of E by Timoshenko's modified beam equation (Eq. 2.23).

Table 3.3 Comparison between the effective modulus computed by the general equation (Eq. 2.10) and by the modified Timoshenko beam theory (Eq. 2.23)

Temperature[°C]	$E_{standart}$[MPa]	$E_{Timoshenko}$ [GPa]
200	196	775
215	97	277
225	32	155
235	27	105
245	21	84

Comparison of both effective modulo (Table 3.3) show that they don't concur. Since it is known that the EB standard equation is not adaptable for this research, Tb has to be modified to be useful. Simulation models have shown that the computed E with Timoshenko's theory above may not be useful for matching displacement from physical to numerical models. In that case the only variable that can be changed is the

correction factor κ. In the initial Eq. 2.23 $k_s = 0.94$ with that value the displacement measured differs to the simulations by a factor of 82 (Table 3.4).

Table 3.4 Comparison of displacement measured and simulated with correction factor $\kappa = 0.94$

Temperature [°C]	Displacement measured [μm]	Displacement simulated [μm]
200	64	78
215	179	219
225	319	389
235	469	571
245	589	720

Previous computations have been performed with the condition $n = 1$ and $\kappa = 0.94$. However, the Fourier series from Wang et al. [20] shows that, with an increase of n and a constant $\kappa = 0.94$, the effective modulus changes with respect to the sinus-function. By using the effective modulus, the measured displacement does not confirm with the simulation results. Therefore, a change has to be done either with an increasing n, or with a different value for the correction factor κ. First, an error calculation has been performed with $n = 1 \ldots 9$ and the results of the measured and simulated displacements were compared to evaluate a useful effective modulus. The results show that with $n = 9$ an effective modulus after simulation is useful to correlate the deflection in the numerical model (Figure 3.8).

Additionally, the same error calculation has been used with different κ values.

To find an accurate correction factor κ multiple simulations with different κ values at a constant temperature $T = 225$°C have been performed. Based on those simulations κ could be determined through an error calculation between the simulation and calculations. Figure 3.9 (a) illustrates the curve of κ at varying values and (b) a detailed view of the narrowed values to determine κ with the smallest error, those values are also listed in Table 3.5.

After comparison of both changes, it can be seen that it is more accurate with a adjustment in κ to confirm with the measured displacement. Fourier series would need to be evaluated more exact to exclude other n values. For the simplified model

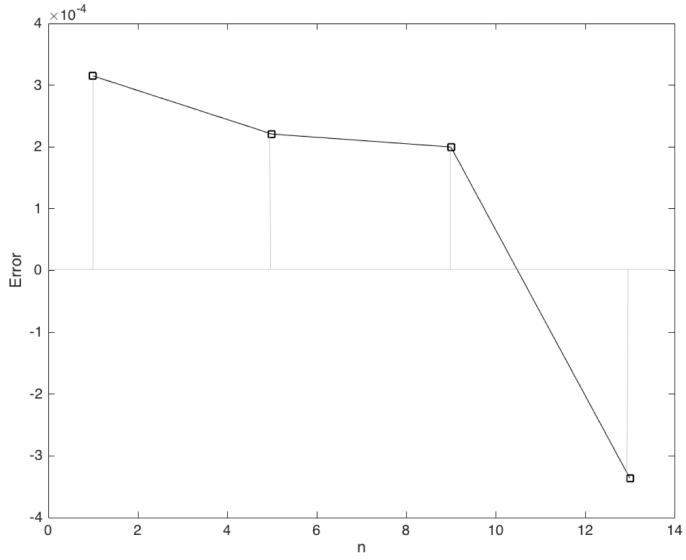

Figure 3.8 Error calculation of multiple n-values to compute an effective modulus to correlate to the numerical model.

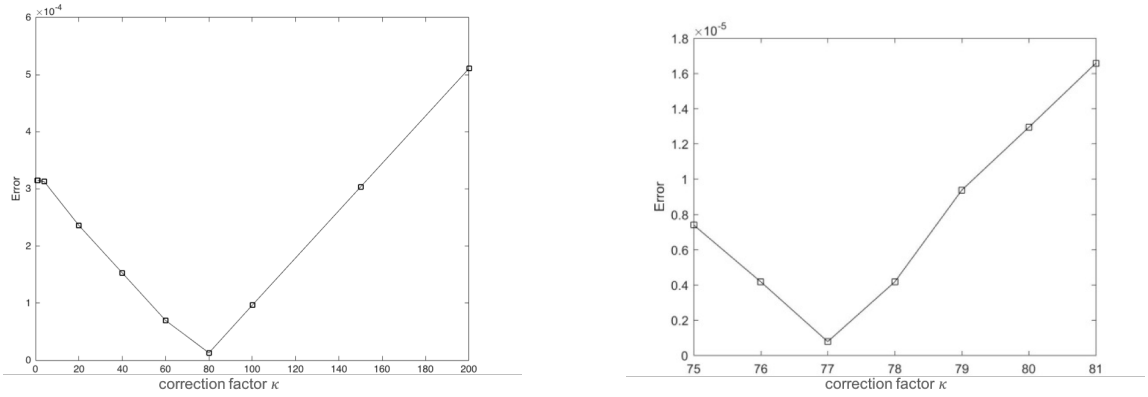

(a) variaty of correction factor κ (b) locolized κ

Figure 3.9 a) A overview of κ values from initial value to an extreme value to localize the smallest error and b) a detailed view of κ with the smallest error pointed out at $\kappa = 77$.

and use in this research the correction which was made and considered for further simulation was, to use $n = 1$ and $\kappa = 77$.

The optimal effective modulus (based on Eq. 2.23) can now be computed with the developed $\kappa = 77$ from above. With this value an alignment between the physical and

Table 3.5 Deflection from physical experiment and simulation with various correc-tion factor values of κ

Temperature [°C]	k_s	Displacement meas. [μm]	Displacement sim. [μm]
225	76	319	315
225	77	319	320
225	78	319	323

simulation model can be achieved. This results in a temperature-dependent effective modulus as it can be seen in Figure 3.10 and Table 3.6.

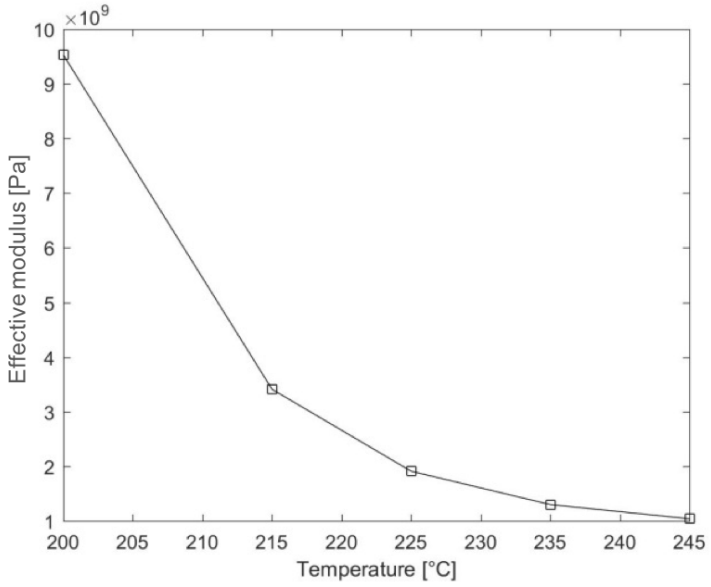

Figure 3.10 Effective modulus over temperature by Eq. 2.23.

Table 3.6 Displacement of one layer strand comparison by measurement and simulation, using Timoshenko's modified beam theory with correction factor $\kappa = 77$.

Temperature [°C]	Effective modulus [GPa]	Displacement meas. [μm]	Displacement sim. [μm]
200	9.53	64	64
215	3.41	179	179
225	1.91	319	320
235	1.30	469	470
245	1.04	589	587

The temperature dependent calculated values for the effective modulus from Table 3.6 are going to be used for all simulations of this model as well as the additional models (Chamfer and self-supporting holes).

3.2.2 Chamfer

Current development of FDM printers show that they are not able to print parts with a parallel overhang surface (0°) to the printing platform without additional support structure. The area will be fully supported, like Figure 3.11b illustrates.

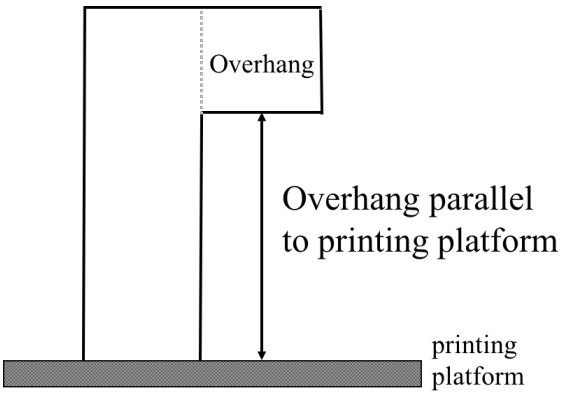

(a) Model description of down-faced overhang prints

(b) expected print illustration

Figure 3.11 Illustration of a model definitions as well as the expected print at a 0° overhang print.

If the user forces printing without support structure, it will cause a drop of layers at the tip (Figure 3.12), depending on the length of the overhang. This shows the defected surface and the need for support. To avoid this issue, designs with 0° overhangs, where sharp transition edges are required should be changed to self-supporting structures. Design features with self-supporting structures can predict the destruction of the down-faced surface. Figure 3.13 displays all three of the considered and analyzed features.

Figure 3.12 Printing failure cause of no support of down-faced parallel areas to the platform at the overhang. As result the tip of each layer drops down.

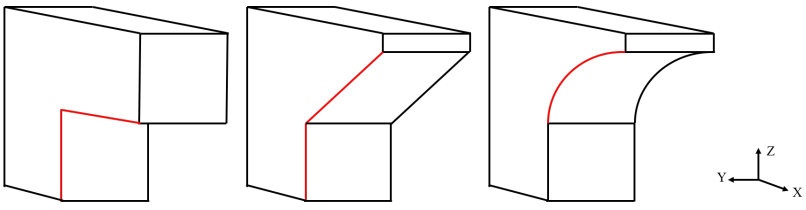

Figure 3.13 Three basic design geometries. (From left: 0° overhang, chamfer and round surface (fillet)).

The concave radius design idea has been merged and is discussed with the self supported hole design in the next section. At the right angle for the chamfer, it is possible to relinquish the support structures and keep the surface quality the same. Other AM methods, such as Selective Laser Melting (SLM), where a laser beam fuses metal powder together, have shown that by decreasing the pitch angle α (Figure 3.14) [16, 17], layers will support themselves.

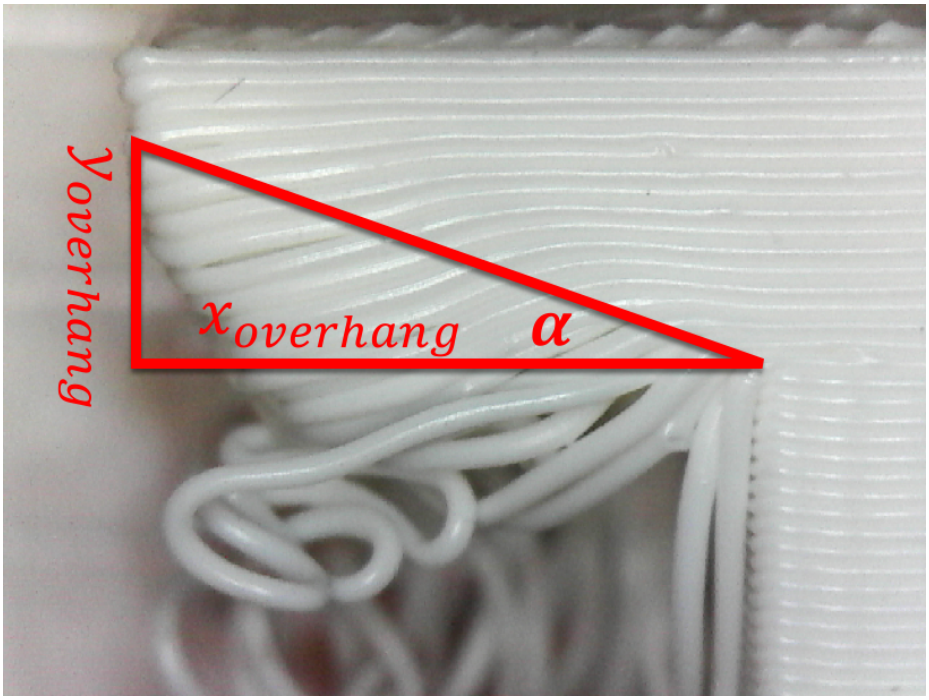

Figure 3.14 Overhang print with visualization of pitch angle α at point of bending at each layer.

This research endeavored to develop design rules for chamfer with a minimum α but an acceptable surface quality. In order to achieve this, the optimal relation between the overhang length ($x_{Overhang}$) and the printing thickness ($y_{Overhang}$), had to be found.

Chamfer Experimental Results

The second experiment in this research was to establish an angle α as small as possible with an adequate surface finish and no support required. To find this angle, prints which failed where analyzed and a similarity of both prints could be observed. If the slope is going to be looked at in detail (Figure 3.15 a) and b)), it can be seen that at a certain point, each layer starts to drop down towards the printing platform. From here a comparison between models have shown that the slope is almost the same and the angle which was found matched almost exactly.

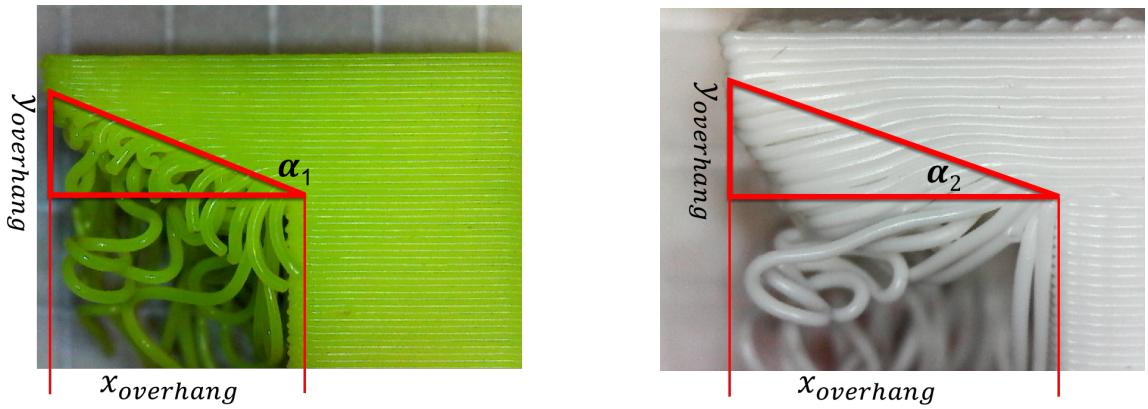

(a) Part 1 with failed overhang and α_1

(b) Part 2 with failed overhang and α_2

Figure 3.15 Two printed overhangs, where the print failed and the layers dropped downwards. It can be noticed that the self-supported layer start dripping at a similar slope.

The pitch angle α is determined for both parts using a 10 mm overhang. For part 1 in Figure 3.14a, the pitch angle is

$$\alpha_1 = \tan^{-1} \frac{y_{overhang}}{x_{overhang}} = \tan^{-1} \frac{3.57}{10} \approx 19.6^\circ, \tag{3.3}$$

and for part 2 in Figure Figure 3.14b,

$$\alpha_2 = \tan^{-1} \frac{y_{overhang}}{x_{overhang}} = \tan^{-1} \frac{3.52}{10} \approx 19.4^\circ. \tag{3.4}$$

Based on these results, parts have been designed and printed with different slope angles α. The fact that α was calculated with 19.6° and 19.4°, parts with a chamfer angle of 15° and 20° where manufactured. In addition, components with an angle of 30°, 45° and 60° (Figure 3.16) where designed to compare the surface structure, especially 45° to the 20°. The angle of 45° is a value, which is clearly established and in any printing software set as a default value. All of the other settings of the print and the printer have been used from the first experiment.

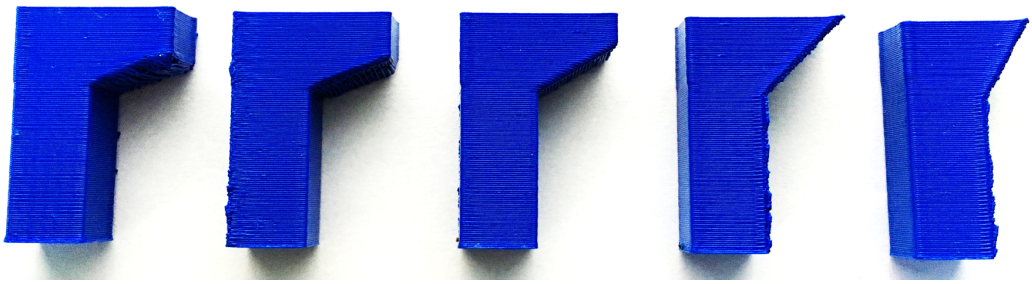

Figure 3.16 Print models with a different slope angle α; from left: 15°, 20°, 30°, 45°, 60°.

The layer thickness (printing diameter) is 0.3 mm and the extrusion temperature $T_{extrusion}$ is kept constant for all experiments at 225°C. At the first print α =15° the tips of the printed layer indicated huge deflections, over 260% of the initial layer thickness. This is also an indication the overhang is to long. Each layer has too much dead load and is not able to support itself. The maximum deflection was measured at this print with $y_{15°}$=0.788 mm and unsupported protruding length of x_0=0.598 mm. Same measurements at α =20° with a surface where each layer still bends at the end but not as much as with a smaller angle. The surface was getting significant better with an increasing α. All measured results, protruding length x_0 and maximum deflection at the tip y_{max} are listed in the Table 3.7 and illustrated in Figure 3.17 below. The exact value of angle α for an acceptable surface structure and no need of sup-port, will be determined in the next chapter. By means of results found and developed

Table 3.7 Parameters (protruding length x_0 and displacement y_{max} for prints with different pitch angle α from 15° to 60°

α [°]	x_0 [μm]	y_{max} [μm]
15	600	790
20	400	350
30	300	230
45	160	63
60	6	13

in this section, a numerical model of parts with an overhang $\neq 0°$ is simulated and the minimal α with its permissible length of overhang x_0 is going to be developed.

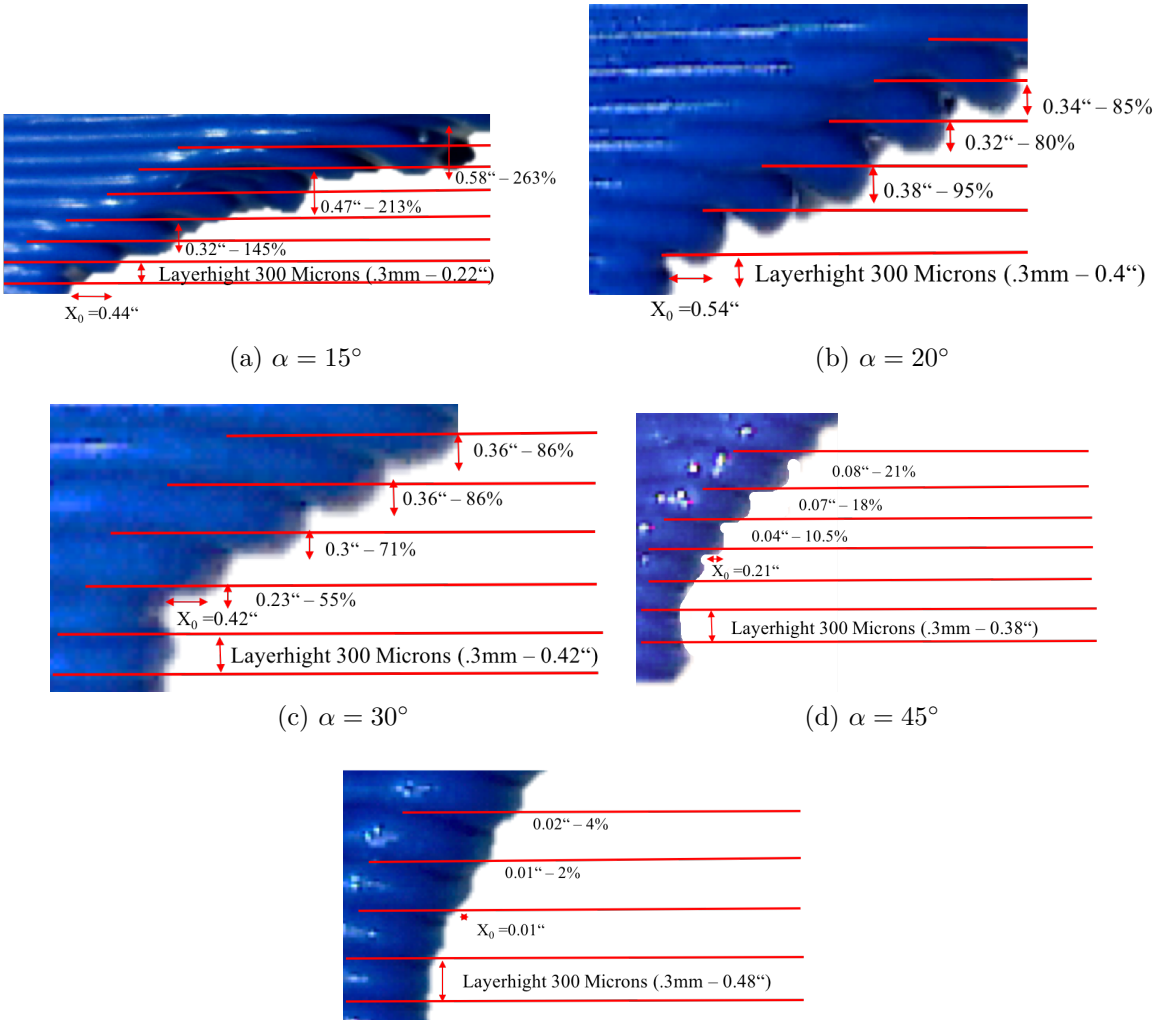

(a) $\alpha = 15°$ (b) $\alpha = 20°$

(c) $\alpha = 30°$ (d) $\alpha = 45°$

(e) $\alpha = 60°$

Figure 3.17 Illustration of various overhang prints with various pitch angle α. Each print with its measures layer thickness, protruding length and max. displacement (measured in inch - mm values can be found in Table 3.7). The pitch angles are from the top to the bottom as follows: 15°, 20°, 30°, 45°, 60°.

3.2.3 Circular Geometry

Circular geometry, in its upright position, is very difficult to manufacture within the FDM process, without support structure. In contrast to the second experiment of printing overhangs (which are open at one side), the support material in holes

sometimes cannot be accessed. If the print layout does not allow part orientation with holes laid down on the platform, support structure is necessary (Figure 3.18).

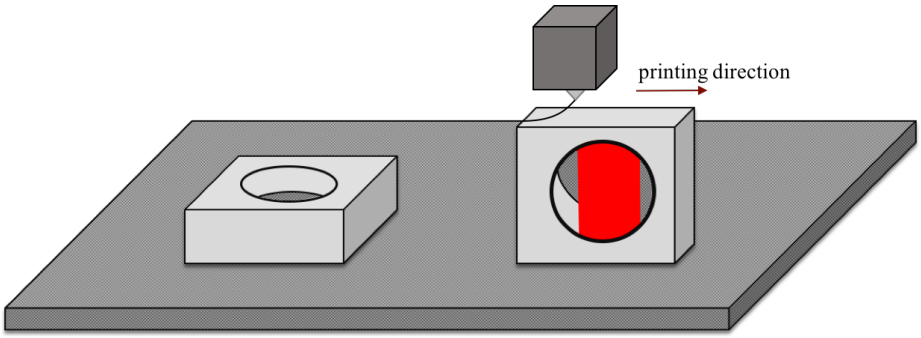

Figure 3.18 Layout of circular geometry on printing platform.

The shape of round holes will not be accurate and the surface shows major defects (Figure 3.19). This will have an effect on further processes or use and cannot be taken into account anymore.

Figure 3.19 Surface of a printed non-supported round hole.

Circular Geometry Experimental Results

Experiments of round holes with difference diameters were printed to see if there is a relation between the hole diameter and the degree of deformation of the surface (Figure 3.20).

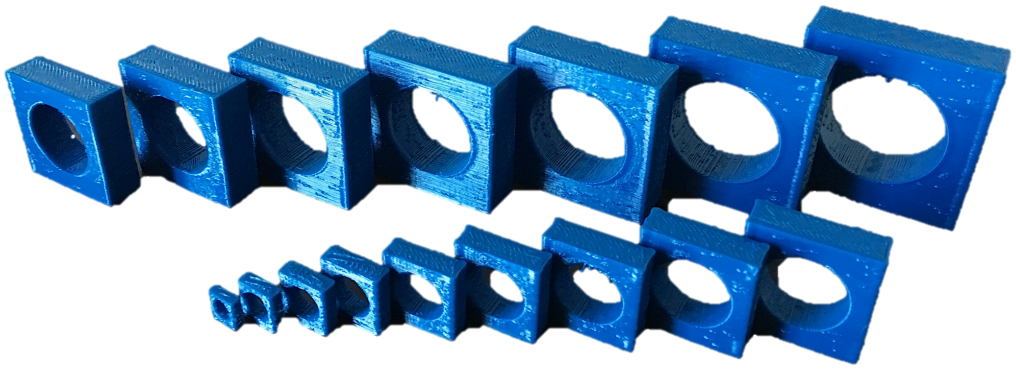

Figure 3.20 Print models of round circular geometry with different diameter.

The result was as expected, as illustrated in Figure 3.21. The diameter of the hole has no major impact on the surface. At the top of the hole where the overhang gets to 0° the printed layer bends down.

Adam et al. [14] has developed design rules for printing holes without support to a certain inner radii r_i. The result of $r_i \leq 5$ mm round holes can be printed without any support structure. This statement was confirmed with the experiments from this research. Significant surface issues appeared at $r_i > 5$ mm. $R_i > 5$ mm will influence the surface of the 0° overhang area also shown in a print result from [14] (Figure 3.22).

Compared to the prints from this experiment it can clearly be seen that with an increasing inner radii r_i, the strands at the overhang surface area are not linked to each other anymore. Figure 3.21a with a $r_i = 5$ mm is confirming the results from Adam et al. [14]. Figure 3.21b with $r_i = 7$ mm already has single strands bending downwards. This effect can be seen in Figure 3.21c,d,e. In Figure 3.21f at $r_i = 35$ mm the surface is so much destroyed that the following layers not bond.

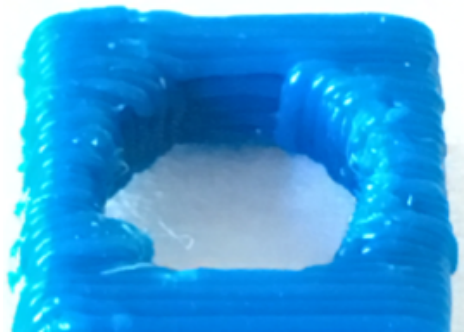

(a) $r_i = 2.5$ mm

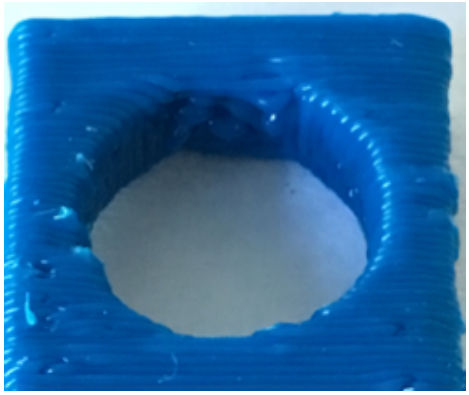

(b) $r_i = 3.5$ mm

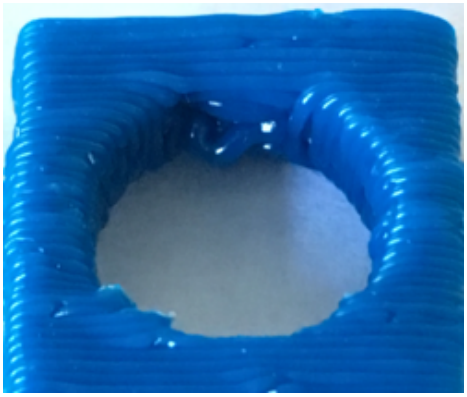

(c) $r_i = 5$ mm

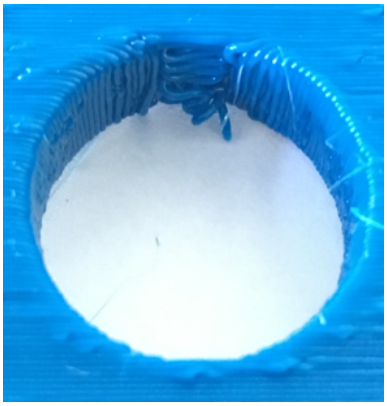

(d) $r_i = 10$ mm

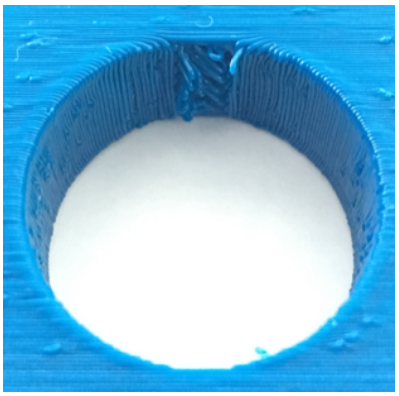

(e) $r_i = 15$ mm

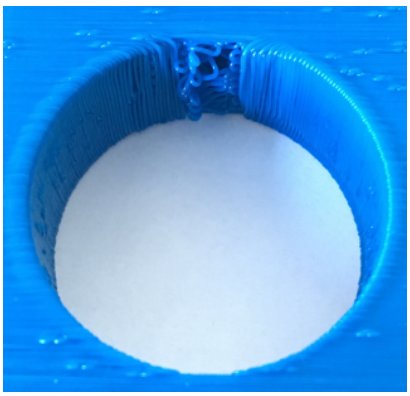

(f) $r_i = 17.5$ mm

Figure 3.21 Illustration of the surface after printing round holes without support structure. The bigger r_i gets the more bending at the 0° overhang area appears

Printing round holes with no support is not acceptable. Therefore, a design approach for FDM printing needs to established. By merging the results from the cham-

Figure 3.22 Result of Adam et al. [14] research about finding the minimum inner radii for round holes with no need of support at FDM prints.

fer experiments with these tests, it is possible to create a design of self-supporting holes. Figure 3.23 shows the design approach with a round hole as base and instead of a 0° overhang at the top, it will overflow in a slope with a minimum angle α as an attachment.

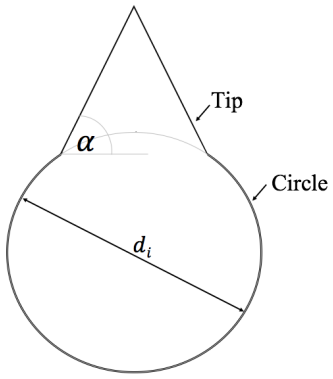

Figure 3.23 Design approach for applying minimum α at the overflow from the circle into the tip.

With use of α as small as possible, it is also possible not to exceed the dimensions of the initial hole too much. To confirm those assumptions, parts have been printed with different diameters r_i and slope angles α, see Figure 3.24.

A detailed view shows that compared to round holes, the surface area at the top is much smoother and no apparent bending occurs. Table 3.8 lists the results of the self-supported design at FDM printing. Figure 3.25 explains where the circular height

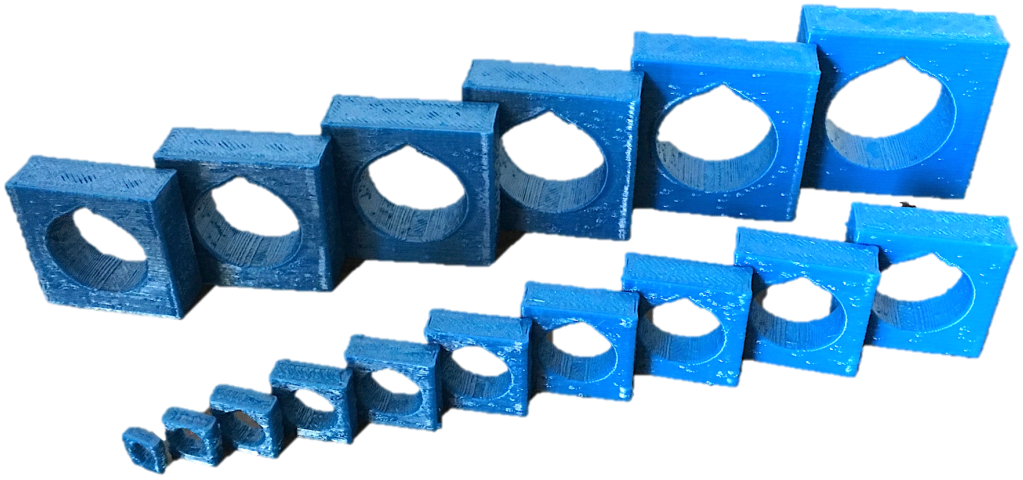

Figure 3.24 Parts for tests with circular and overhang geometry combined.

is being measured for better understanding. Figure 3.26 gives an overlook of some printed examples and the surface structure of the slope area.

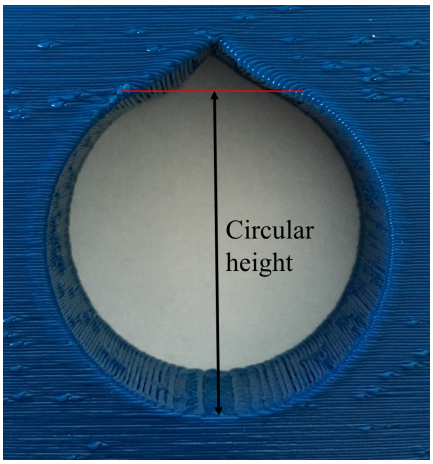

Figure 3.25 Explanation of measured distance of circular height.

Table 3.8 Measurements of prints from merging two geometries with a diameter from 5 mm to 36 mm and an overflow angle $\alpha \approx 30°$

Circular ⌀ [mm]	Tip [mm]	Circular height [mm]
5	0.3	4.7
7	0.5	6.5
10	0.7	9.3
12	1	11
14	1.3	12.7
16	1.5	14.5
18	1.7	16.3
20	1.8	18.2
22	2.1	20.9
24	2.3	21.7
26	2.5	23.6
28	2.6	25.4
30	2.8	27.2
32	3.1	28.9
34	3.3	30.7
36	3.4	32.6

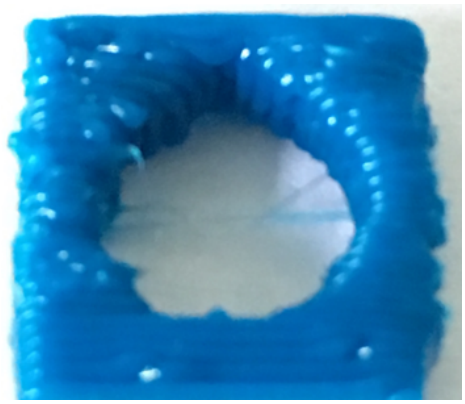

(a) $hole_{diameter} = 5$ mm

(b) $hole_{diameter} = 7$ mm

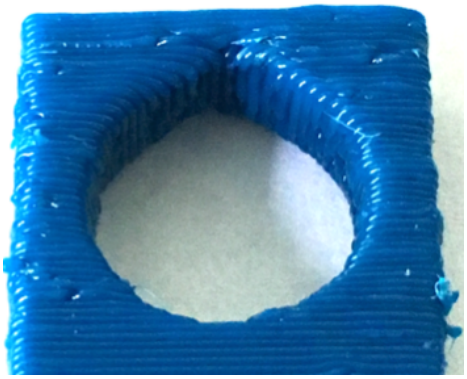

(c) $hole_{diameter} = 10$ mm

(d) $hole_{diameter} = 15$ mm

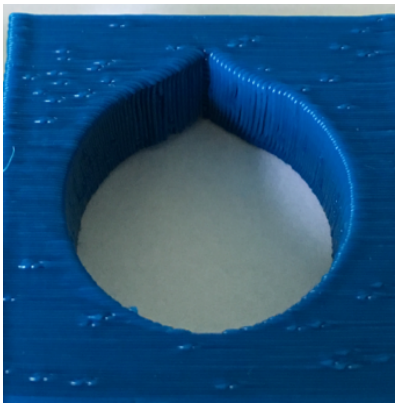

(e) $hole_diameter = 20$ mm

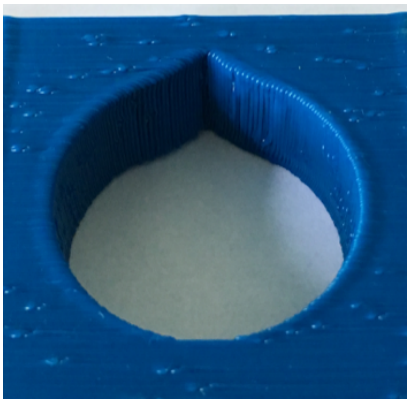

(f) $hole_{diameter} = 30$ mm

Figure 3.26 Illustration of the surface after printing round holes without support structure. The bigger r_i gets the more bending at the 0° overhang area appears.

3.3 Comparison to Analytic Model

Compared to the analytic model, Timoshenko's beam theory was modified and adapted and used for verification of the physical experiments. The results did match

the before computed results by using the developed equations. The first experiment, single strand laid the foundation for all further calculations. By developing the effective modulus with physical experiments, more complex computations for overhangs and other designs where realized. The analytic model is dependent on a correction factor κ, which also was developed by the physical experiments. Every experiment was able to match the established equations and confirmed the predictions, which where made. The last experiment is a mix between a design approach of a minimum slope angle α beforehand and previously unattainable round hole design. When combined, it is possible to print a model that is self-supporting and with the small angle α the maximum height of the hole will not be exceeded too much.

4. NUMERICAL MODEL OF 3D PRINTED PART FEATURES

In the following chapter, the modeling methods and theories which have been reviewed in Chapter 2 and 3 as well as parameters of the numerical model and settings are presented. Figure 4.1 shows a flow chart of the procedure ,in ANSYS, for simulating the models. Afterwords each physical experiment has been simulated and validated with the analytic results.

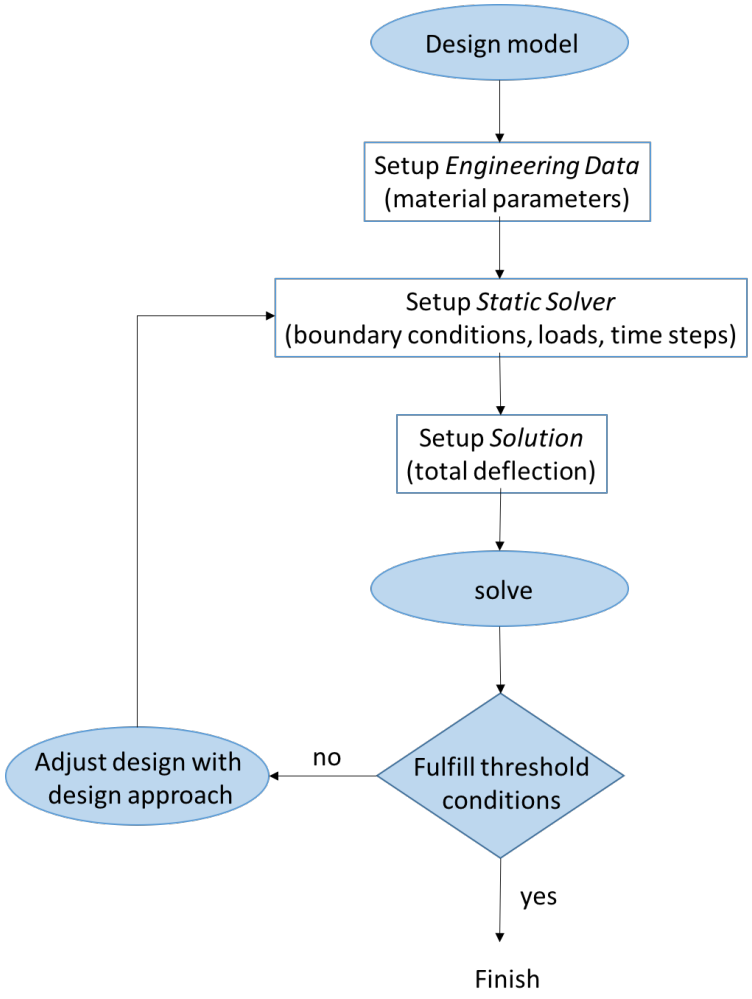

Figure 4.1 Flow chart for the procedure of the numerical model.

4.1 Model Calibration and Conceptual Model Error

Model calibration is the process of model adaptation to a reference system. This can be achieved through the setting parameters by several samples from the reference system. This can be achieved through the setting of parameters by several samples from the reference system. Model calibration is useful for complex simulation models compared to experimental equivalent models. With the developed equation for the effective modulus E, Eq. 2.23 and the measured deflection from the physical experiments in Chapter 3, parameters for the numerical model can be determined. It has been seen that simulation with a low value of the effective modulus at a high temperature is a rather conservative result which will be more noticeable in complex models than at one single strand simulation. All models have been simulated at the same constant temperature to be comparable. The first two validations (single strand and chamfer) have been carried out with the temperature of extrusion $T = 225°\text{C}$ to have a numerical model that is matching with the tests for further more conservative analysis. It has been known that different temperature areas occur in the part (again more noticeable at complex parts). For the research and validation of the effective modulus and the deflection at single layers, it was valid-enough. The environmental temperature is the temperature in the chamber of the MakerBot and has influence in the cooling down time of ABS. In Table 4.2 we summarize the temperature settings, which had been used for each simulation.

Table 4.1 Parameter settings for numerical models for validation of the analytic model and the physical experiments

	Temperature [°C]	Effective modulus [GPa]
Single strand model	225	1.91
Chamfer model	225	1.91
Circular geometry model	245	1.03

4.2 Verification of Numerical Model

4.2.1 Single String

Simulations of one single strand validate the physical experiments and analytic calculations and develop the temperature dependent Young's modulus. Multiple experiments were printed (explained in Chapter 3) and those parts were simulated at defined boundary conditions. The calibration for this model was a variable $E(T)$ as well as fixed supports at the strand on both ends. The force applied was the body force w, uniform over the strand. All necessary parameters for each model in the material data or the model are listed below in Table 4.2

Table 4.2 Parameter setting for numerical model of one single strand at a various temperature

Temperature [°C]	Effective modulus [GPa]	Uniform load [$\cdot 10^{-4}$ N/m]
200	9.53	7.489
215	3.41	7.489
225	1.91	7.489
235	1.30	7.489
245	1.04	7.489

The following figures show the results of all five simulations on ANSYS Workbench. All simulations have the same measurements as the actual prints.

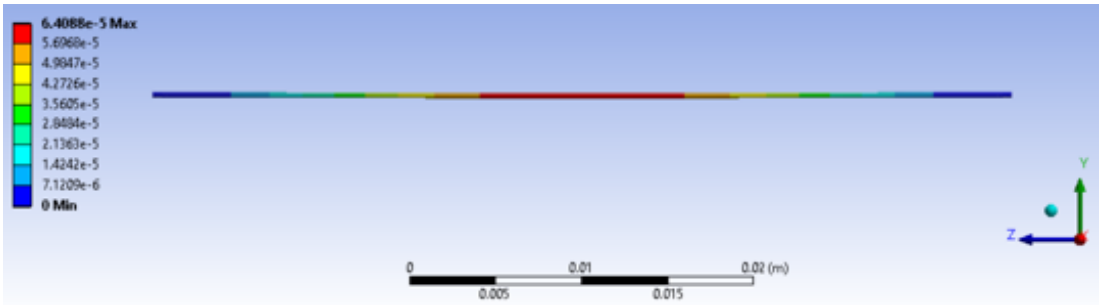

Figure 4.2 Simulation of a single strand at 200°C and $E(T) = 9.53$ GPa.

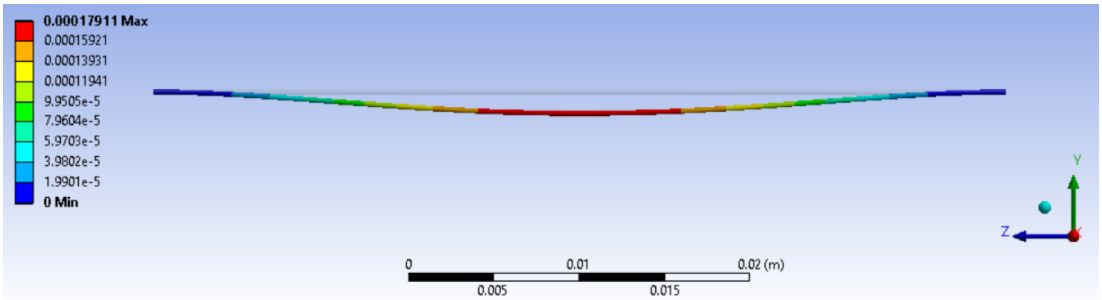

Figure 4.3 Simulation of a single strand at 215°C and $E(T) = 3.41$ GPa.

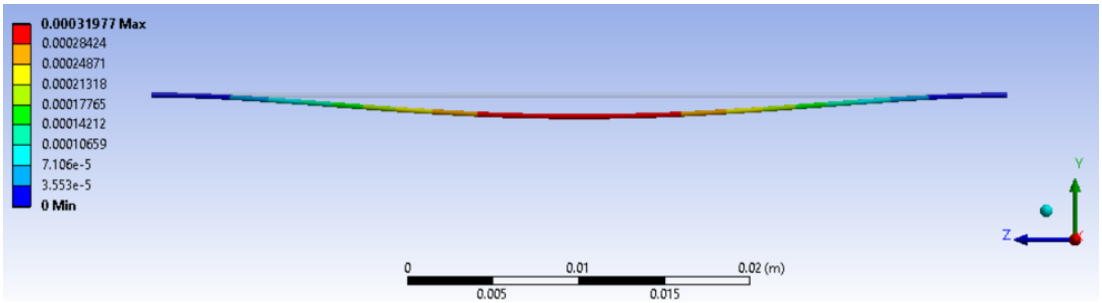

Figure 4.4 Simulation of a single strand at 225°C and $E(T) = 1.91$ GPa.

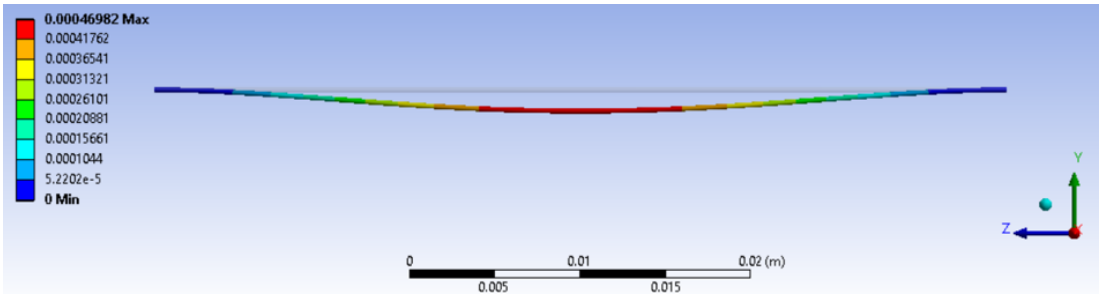

Figure 4.5 Simulation of a single strand at 235°C and $E(T) = 1.30$ GPa.

In Table 4.3 we list deflections of the physical experiment compared to the numerical model, established with $E(T)$ and w from Table 4.2.

Comparison to Analytic and Physical Results

If the results from the analytic derived calculations as well as the prints with the simulation are being compared, results are confirmed with finite element anal-

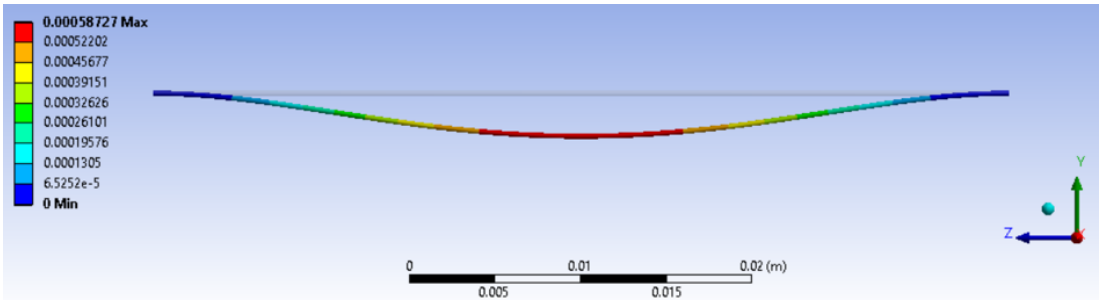

Figure 4.6 Simulation of a single strand at 245°C and $E(T) = 1.04$ GPa.

Table 4.3 Comparison between the experimental and simulated maximum deflection at the center of the strand.

Temperature [°C]	Deflection measurments [μm]	Deflection simulation [μm]
200	64	64
215	179	179
225	319	320
235	469	469
245	589	587

ysis. With measurements of the maximum deflection at the prints, it was possible to compute a effective modulus through previously developed equations. For simulations and predictions of the behavior of more complex prints it is necessary that the simulation match with the actual prints. This can be achieved with the earlier determined temperature dependent effective modulus. Neither environment temperature was considered. The latter of the two factors influences on the cooling time of the material.

4.2.2 Chamfer

By reviewing literature about printing overhangs, it can be found that the most common printing angle α is 45° at FDM printing. Experimental prints in Chapter 3, showed that printing a 0° overhang of 10 mm leads to an unpredictable drip of the first couple overhang layers (refer to Figure 3.11).

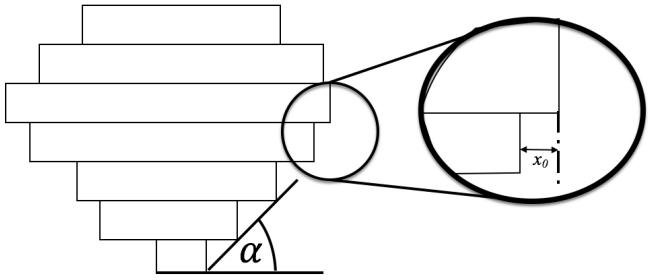

Figure 4.7 Illustration of printing angle α and layer overhang x_O.

During those experiments it indicates that a slope can be seen to the layer above that support one slope vs. several slopes. Different angles have been printed (Figure 3.15) and simulated to find an optimal x_O where layers support themselves to minimize the support underneath. Below we have displayed all five models with different overhang lengths simulated at the same temperature of $T_{Extrusion} = 225$°C to compare the simulations with each other.

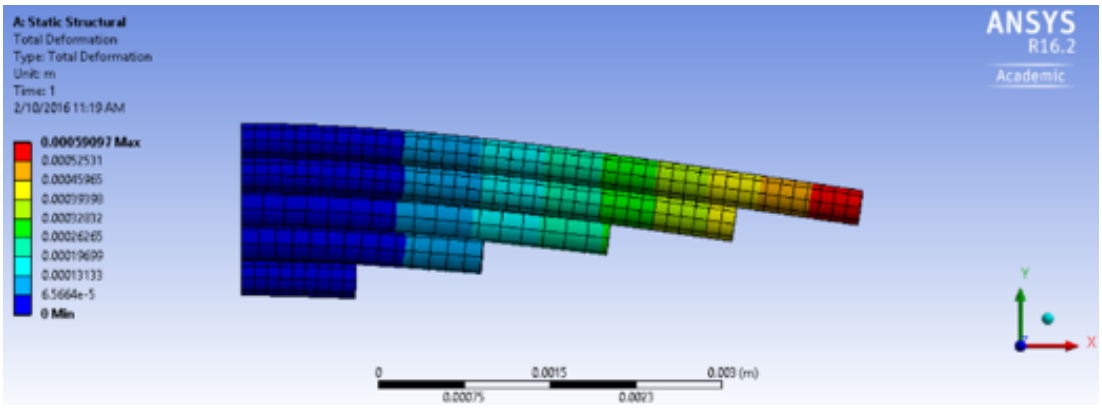

Figure 4.8 Simulation of $x_O = 0.598$ mm overhang and $\alpha = 15°$.

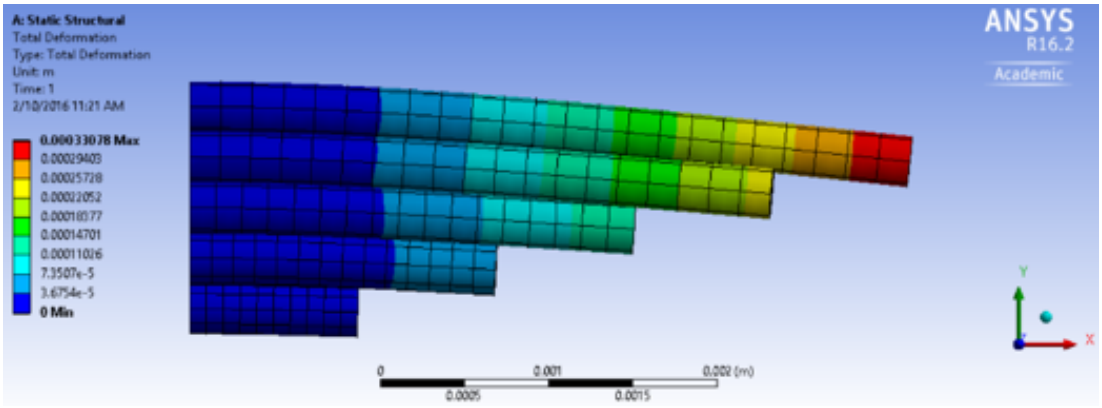

Figure 4.9 Simulation of $x_O = 0.405$ mm overhang and $\alpha = 20°$.

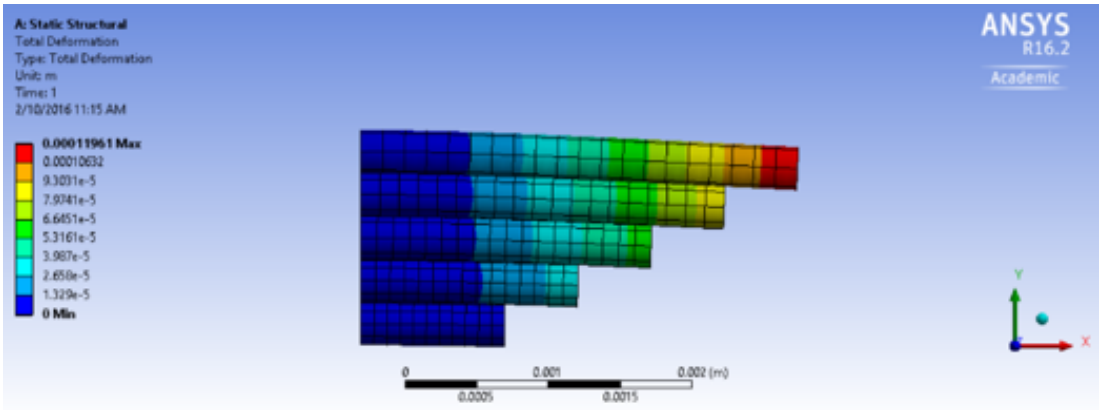

Figure 4.10 Simulation of $x_O = 0.298$ mm overhang and $\alpha = 30°$.

Comparison to Analytic and Physical Results

Previous calculations and simulations provided the effective modulus, which now was applied to those simulations. After simulating the first five layers of each model and considering a factor of safety 1.4, the measured deflections from the models nearly matched the deflections from the simulations (see Table 4.3)

The small difference in the 3D prints is due to various environmental temperatures, which cannot be taken into consideration for simulations, as well as the exact

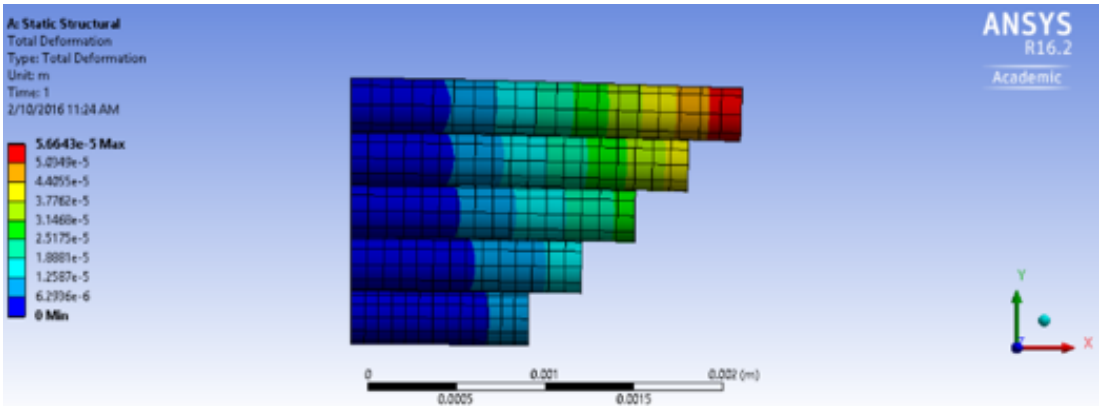

Figure 4.11 Simulation of $x_O = 0.165$ mm overhang and $\alpha = 45°$.

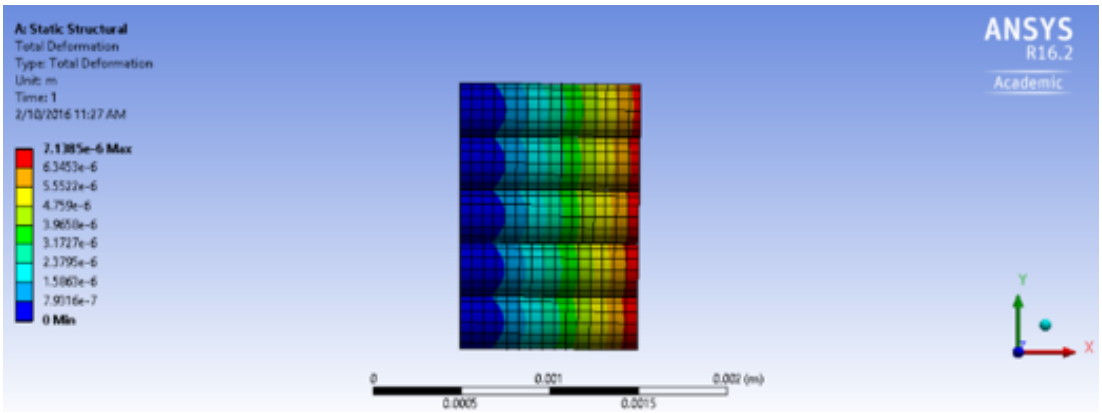

Figure 4.12 Simulation of $x_O = 0.006$ mm overhang and $\alpha = 60°$.

composite and properties of ABS. Given an applied uniform load, the permissible length of each overhang length x_O is given by

$$x_O = \frac{d}{tan(\alpha)}, \tag{4.1}$$

where d is the filament diameter and α the overhang angle. For $d = 300\mu$m and $22° \leq \alpha \leq 27°$, one obtains that 742μ m $\leq x_O \leq 588\mu$m.

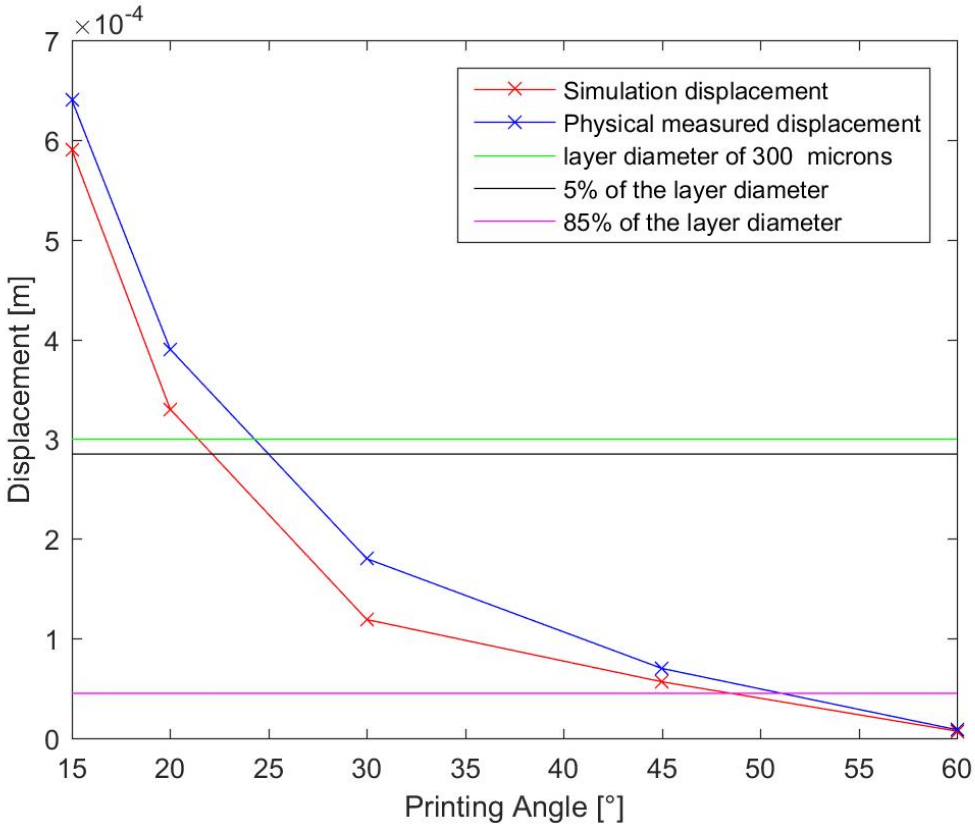

Figure 4.13 Comparison of measured and simulated displacement over overhang angle.

At the point of intersection in Fig. 4.13, it can be observed that the displacement is less than 5% of the layer diameter. Also, the deflection is less than 5% and negotiable. Notably, most commercial 3D printing systems use a boundary of overhang angle at 45°. It can be seen in the diagram that the deflection is close to zero compared to the layer diameter and in that case is negligible. Because of a small variation between deflection and printing diameter, 45° is the most frequent overhang angle. In our study it can be found out that using a 5% deflection offset, the overhang angle α can be reduced to 22° to 27°.

4.2.3 Circular Geometry

Experiments have shown that the surface of a circular geometry will be defected when printed without support at the overhang. Those examples have been simulated as well. Since it is a more complex structure the parts before the simulations were executed with the highest extrusion temperature $T_{Extrusion} = 245°C$. Simulating at this temperature will lead to a effective modulus of $E = 1.03$ GPa, which is the most elastic scenario in this case. The simulation with these parameters are chosen very conservatively to develop a numerical model that is accurate enough to predict deflection areas without considering all temperature zones. Influential factors such as environmental temperature and platform heating temperature were not considered in the numerical model.

Below are all simulation models from the circular geometry with a changing diameter of the center hole. Underneath those simulations, parts with a self-supported structure are simulated, also with a variety of different diameters and tip heights (explained in Chapter 3).

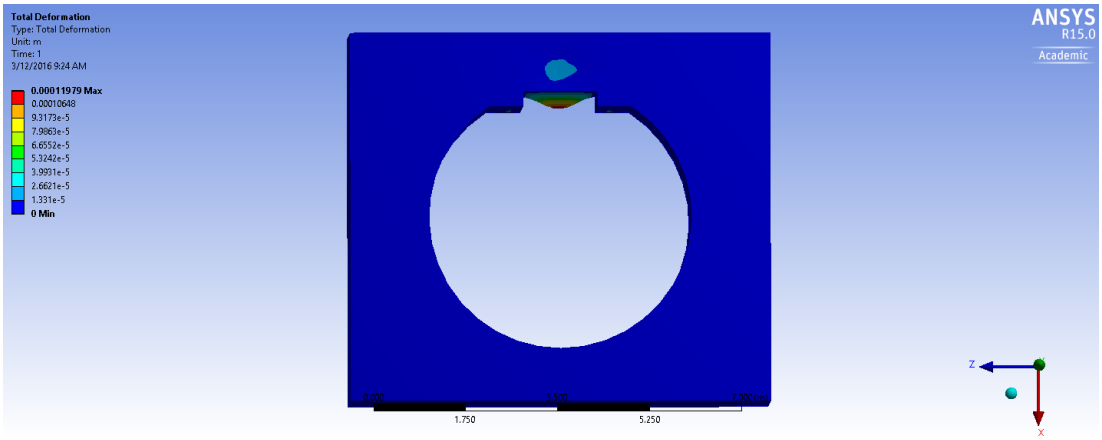

Figure 4.14 $hole_{diameter} = 5$ mm and a overhang $y_{max} = 0.119$ mm.

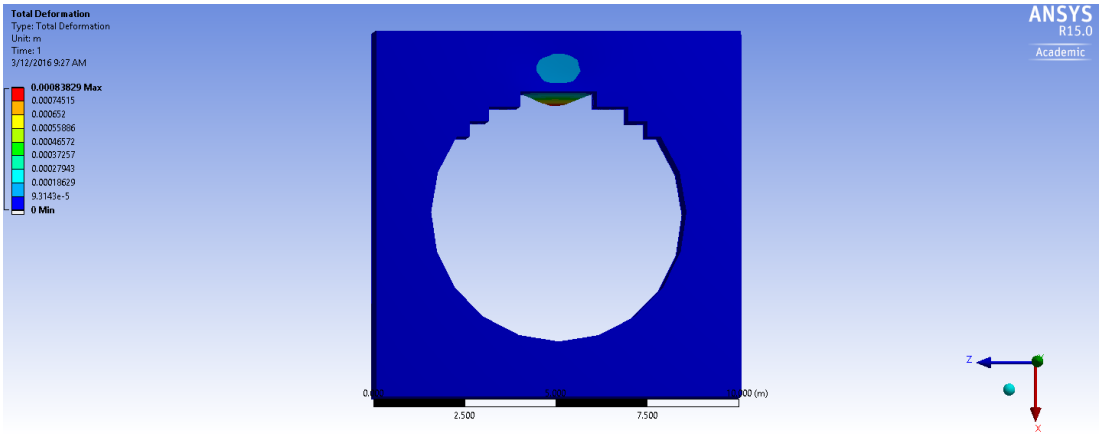

Figure 4.15 $hole_{diameter} = 7$ mm and a overhang $y_{max} = 0.838$ mm.

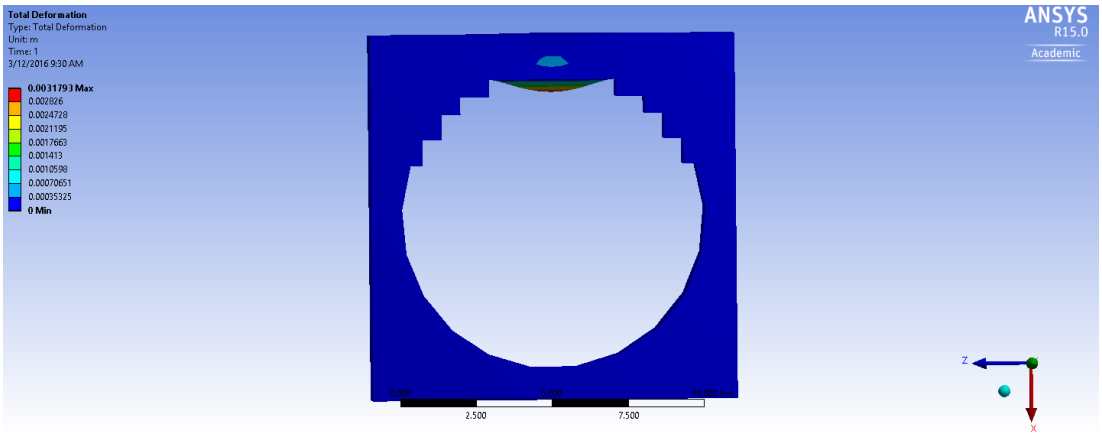

Figure 4.16 $hole_{diameter} = 10$ mm and a overhang $y_{max} = 3.17$ mm.

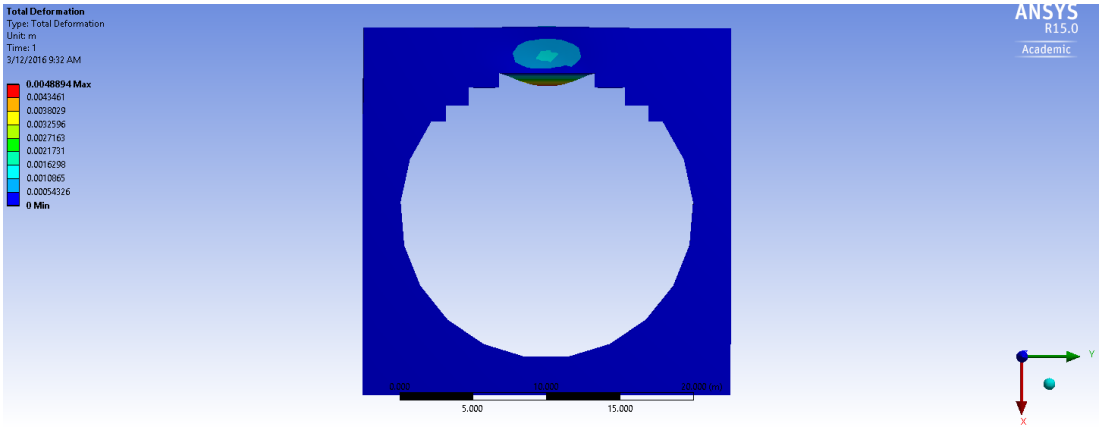

Figure 4.17 $hole_{diameter} = 20$ mm and a overhang $y_{max} = 4.88$ mm.

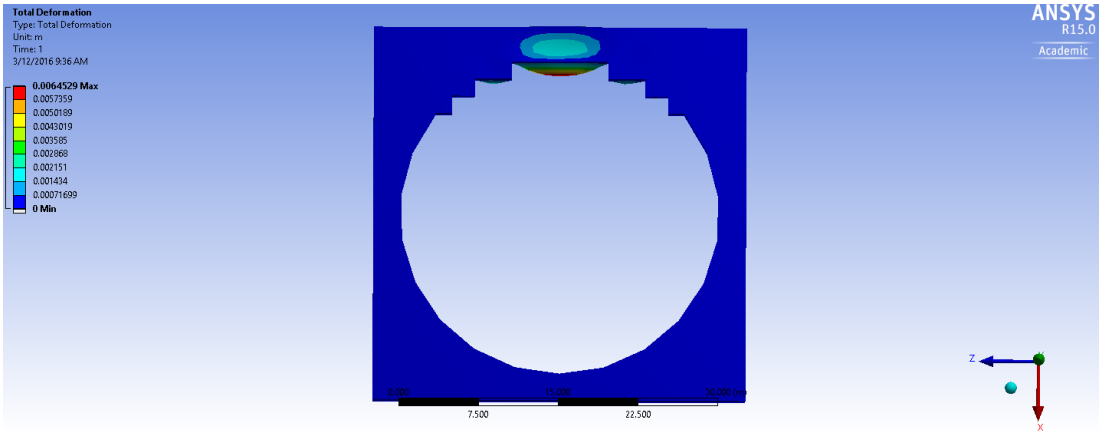

Figure 4.18 $hole_{diameter} = 30$ mm and a overhang $y_{max} = 6.45$ mm.

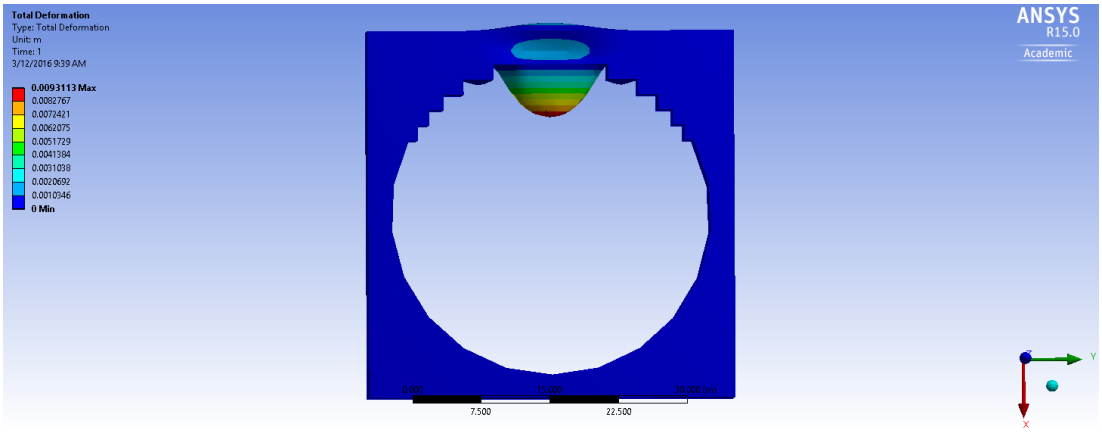

Figure 4.19 $hole_{diameter} = 35$ mm and a overhang $y_{max} = 9.31$ mm.

Following are simulation results from self-supported design models:

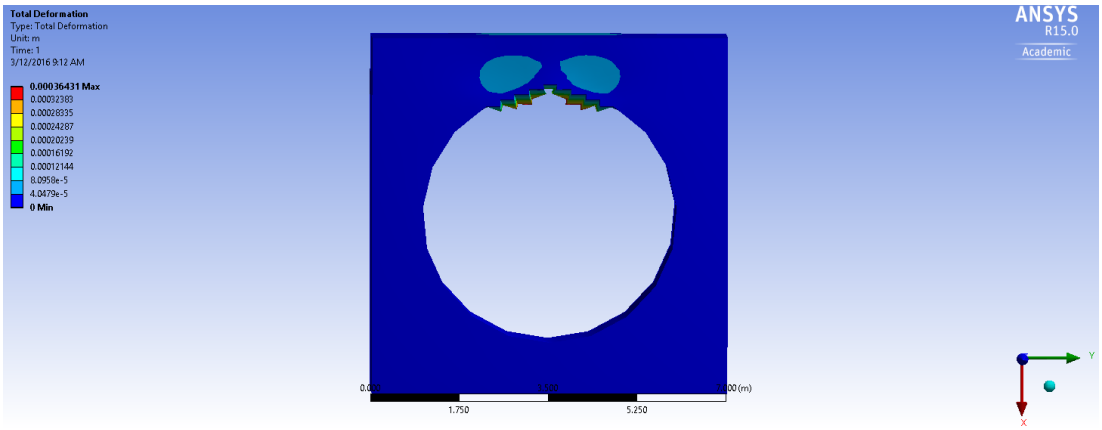

Figure 4.20 Self-supported design with $hole_{diameter} = 5$ mm, $tip = 0.3$ mm and $y_{max} = 0.36$ mm.

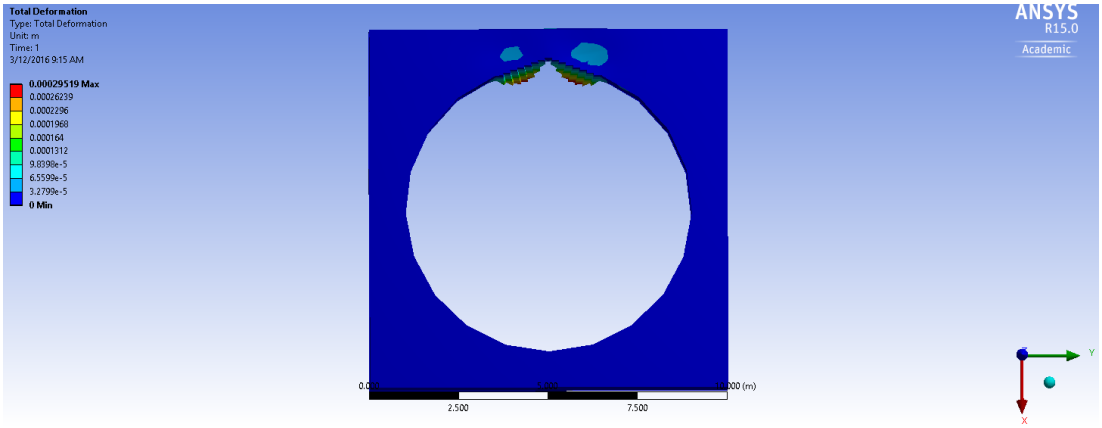

Figure 4.21 Self-supported design with $hole_{diameter} = 7$ mm, $tip = 0.5$ mm and $y_{max} = 0.29$ mm.

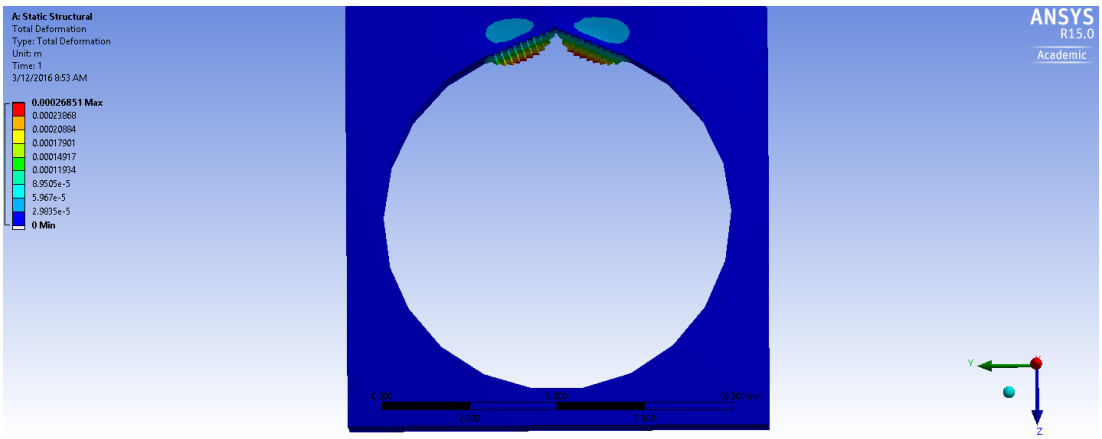

Figure 4.22 Self-supported design with $hole_{diameter} = 10$ mm, $tip = 0.7$ mm and $y_{max} = 0.26$ mm.

4.3 Comparison to Analytic and Physical Results

The simulations of the circular geometry model over predicts the deflection at the 0° surface area. Compared of the experiments with a broken surface at 0°, the simulations are matching the deflection, when simulated at a temperature $T = 245$°C and a effective modulus $E = 1.03$ GPa. A relation between the $hole_{diameter}$ and 0°-overhang-length can be noticed with an increasing overhang the deflection of the lower exposed layers increase as well. The follow up layers will be supported because

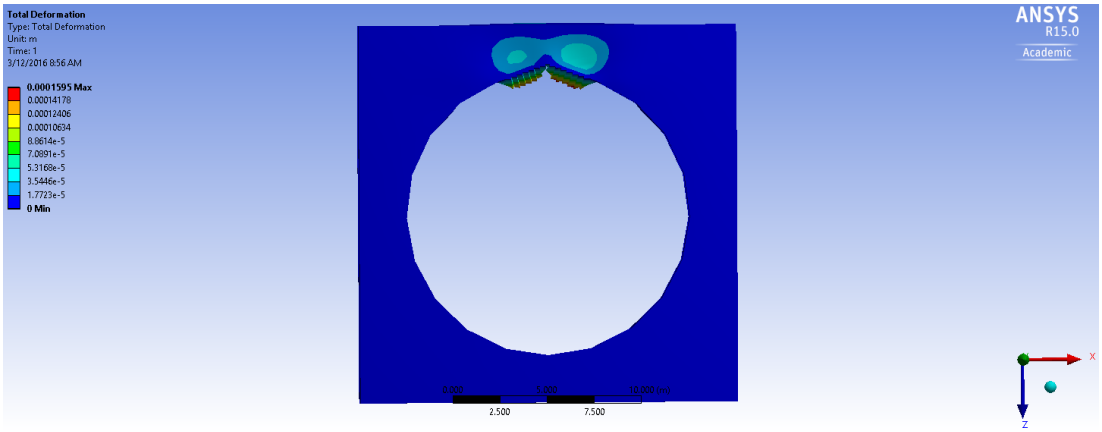

Figure 4.23 Self-supported design with $hole_{diameter}$ = 15 mm, tip = 1 mm and y_{max} = 0.15 mm.

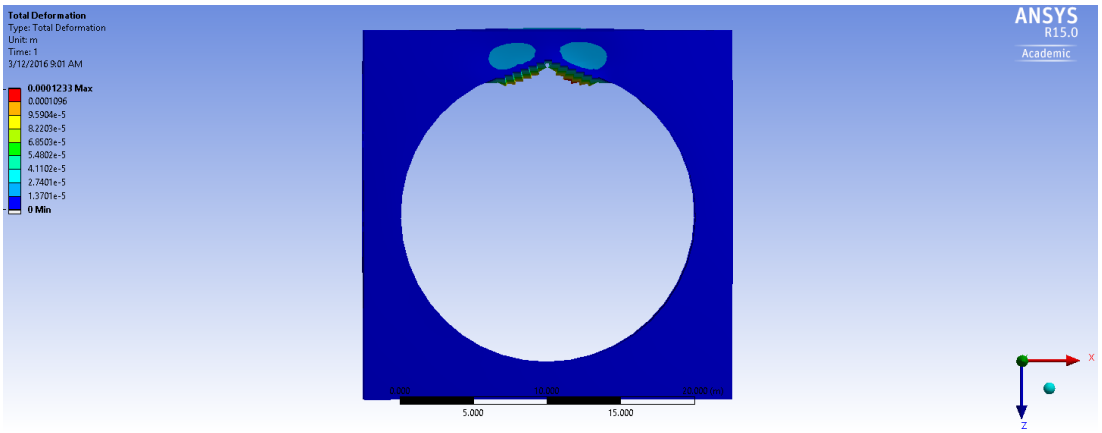

Figure 4.24 Simulation of printed self-supported design with $hole_{diameter}$ = 20 mm and tip = 1.3 mm with a maximum predicted deflection of y_{max} = 0.12 mm.

of cooling down from the layers underneath. Changing the initial design of the part to a hole with a tangential tip, the overhang length x_O will be reduced and the layers are able to support themselves right after they print before they can drip. Those design changes are duplicated from the results found at the simulations of a chamfer design in Section 4.2.2. The simulations with the developed parameters form the analytic model are very conservative but predict and verify what can be seen from the printed experiments in Section 3.2.3.

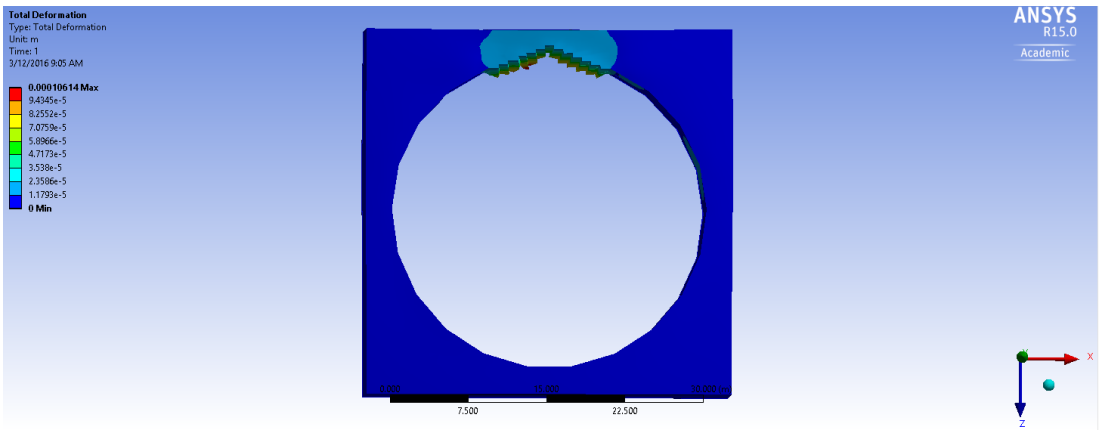

Figure 4.25 Self-supported design with $hole_{diameter} = 30$ mm, $tip = 1.5$ mm and $y_{max} = 0.1$ mm.

5. CASE STUDY: DFAM FOR A TOPOLOGY OPTIMIZED COMPONENT

5.1 Design Approach

The purpose of this case study is to prove that the developed equations of Timoshenko's modified micro structure beam theory in Chapter 2 can be used for numerical models to predict the deflection of complex designs. Dr. Tovar has developed an application for topology optimization in MATLAB and this study will show how the application in association with established design rules of physical experiments can lead to a simulation model to predict the necessary support for very complex designs.

The following section in this chapter presents the initial design, implemented in MATLAB. Then the issue on the topology optimization design is stated and the re-designed part is presented, through applying the design changes. Both designs are simulated in ANSYS to detect defected surfaces and predict the deformation of overhangs. Finally, both designs are compared to each other, numerical as well as with physical prints.

5.2 Optimizing the Design

Optimizing the design for this research, Dr. Tovar's MATLAB GUI for 2-D topology optimization was used. It provides the steps for changing the design from its initial to an optimized design.

Topology optimization creates an efficient design, which meets certain requirements for parts. Maximum stresses and loads on the component is taken into account and a given space in which the part is being optimized. This space is divided into the following three areas: a void, solid, and support area. The void area is the free area, solid is the non-design space, and the support area as the optimization region, see Figure 5.1.

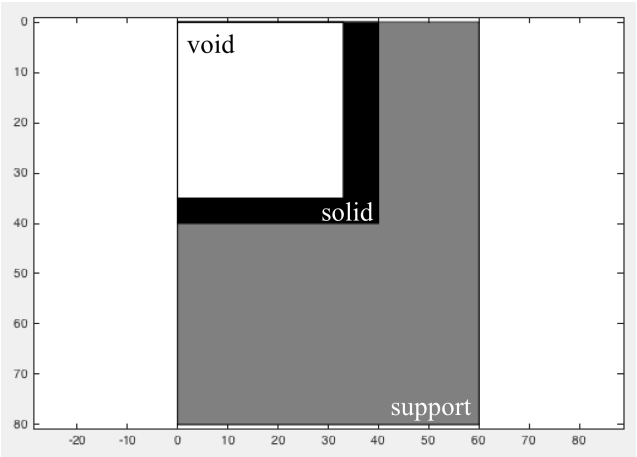

Figure 5.1 Definition of the design space.

Dr. Tovar's MATLAB GUI application generates optimized geometries from two initial geometries, a rectangle or an ellipse. Loads and supports need to be defined for optimally determined stiff and lightweight structures in the support area. For this case study two load cases (LC) were considered. First load case is where a person is going to sit on the chair without leaning back (LC1). The second load case is where the person sits on the chair but also leans back and a force is applied at the back of the chair (LC2). Supported is the chair at the bottom surface in both load cases.

The initial design idea with a full material block underneath the seating area is not efficient for printing (Figure 5.3). As such, topology optimization is necessary by the same performance of the part. The optimization process is displayed in Figure 5.4a to 5.4d.

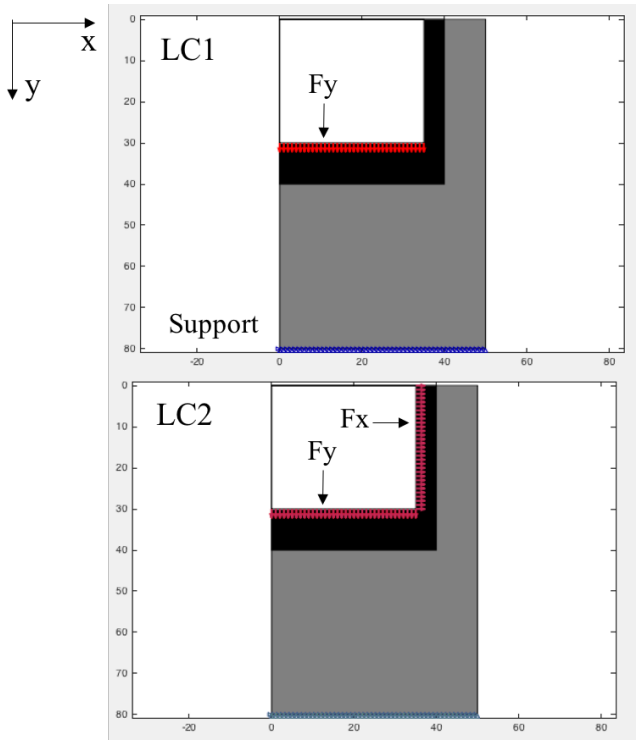

Figure 5.2 Illustration of both load cases in the case of a chair considered the person is only sitting (top:LC1) and the person not only sitting but also leaning back (bottom:LC2) with both times full support at the bottom.

Figure 5.3 Initial design approach of a chair printed with 100% support underneath the seating area.

5.3 Design Analysis

Following subsection will analyze the initial design approach from the topology optimization application as well as the modified design with applied design rules. Both models are simulated and printed for further verification.

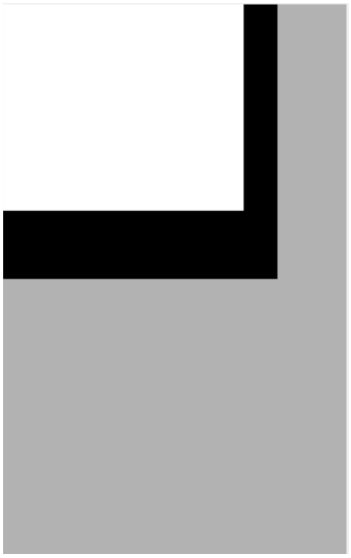

(a) Initial design with 100% support material.

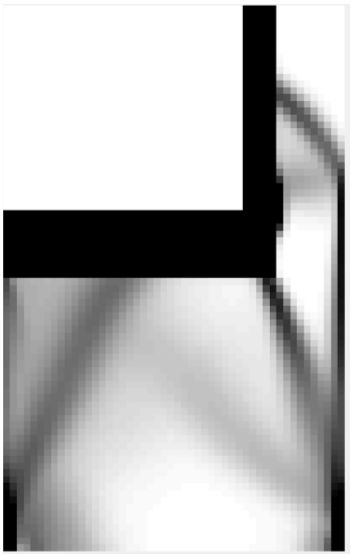

(b) Optimized design with 70% support material.

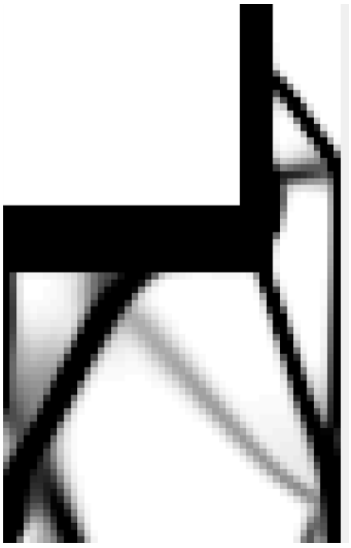

(c) Optimized design with 50% support material.

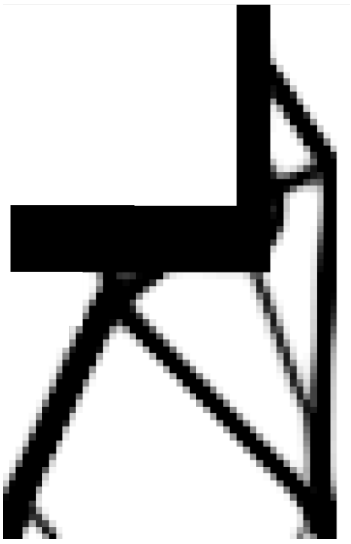

(d) Final optimized design with 30% support material.

Figure 5.4 (a)-(d) Illustration of the topology optimization process from 100% to final 30%in a low-resolution. The final design will give the best distribution of material withing the design domain to fulfill both load cases.

5.3.1 Simulation of the Initial Design Approach

For simulating the model, the optimized design needs to be created as a printable part, see Figure 5.5.

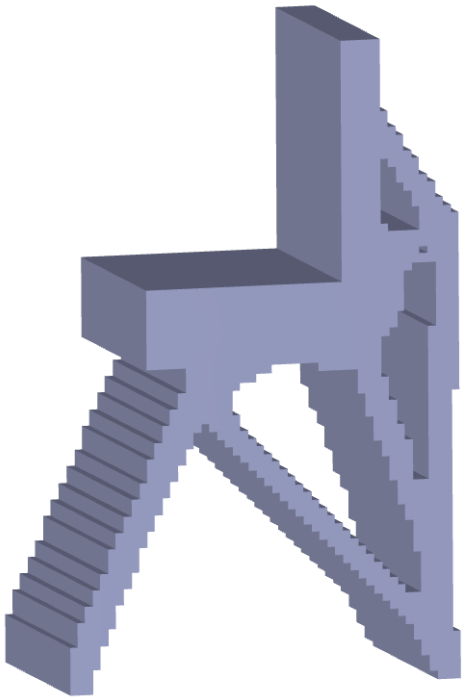

Figure 5.5 CAD model of the image from the MATLAB GUI application of the initial topology optimization.

This model can be implemented into ANSYS Workbench and simulated like the other experiments, explained in Chapter 4. Parameters were determined more conservatively in order to predict the most deflection of the part and simulate the worst case. The simulating printing temperature has been chosen with $T_{Extrusion} = 245°\text{C}$ and a effective modulus $E = 1.03$ GPa. The results are illustrated in Figure 5.6.

Deflection occurs at the faces oriented downward toward the printing platform. The deflection confirms the results, which where developed from the other experiments. The over predicted deflection $y_{max} = 1.2$ mm is shown as red (problematic) areas of the design. Resulting from the simulation and the many 0° overhangs, it can be said that printing this design would lead to a full supported design. The design needs to be modified in order to reduce support.

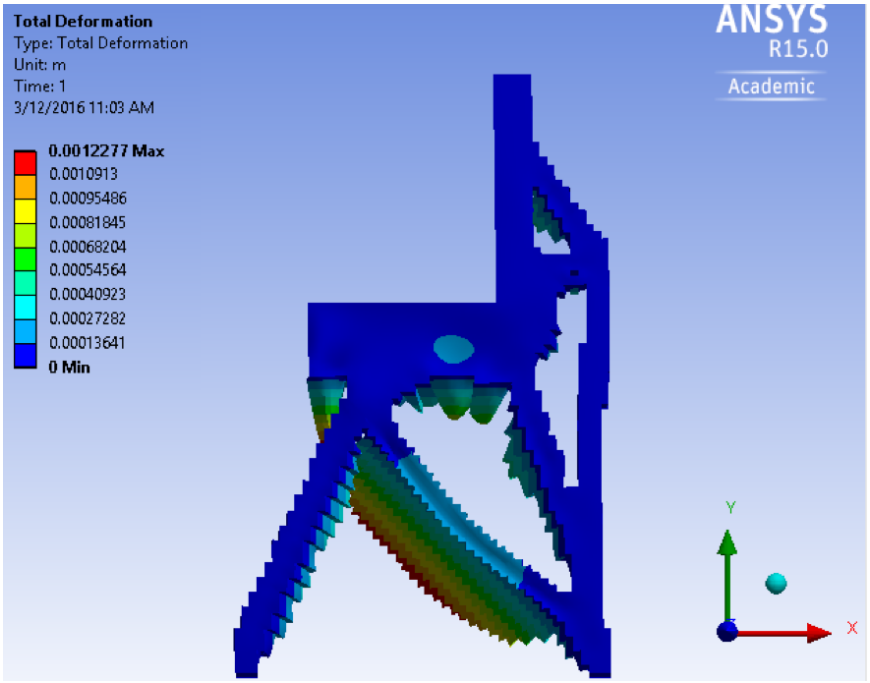

Figure 5.6 Simulation to predict the deflection of the topology optimized design with low-resolution

5.3.2 Applying Design Rules

The first optimized design is a result of a low-resolution direct implemented design from the MATLAB GUI application. To prevent the 0° overhangs the design is changed to more high-resolution design, which means that all 0° overhangs that are ≤ 0.2 mm are being changed to a straight line (Figure 5.7). All larger overhangs are kept the same. The second change which was applied where to add a chamfer with a pitch angle of 25° to it (Figure 5.8) In Figure 5.9 are both designs compared, the initial low-resolution design as well as the modified chair design.

The final design will look like it is shown in Figure 5.9. The CAD model, created from the previous developed design rules, has been used for further simulation.

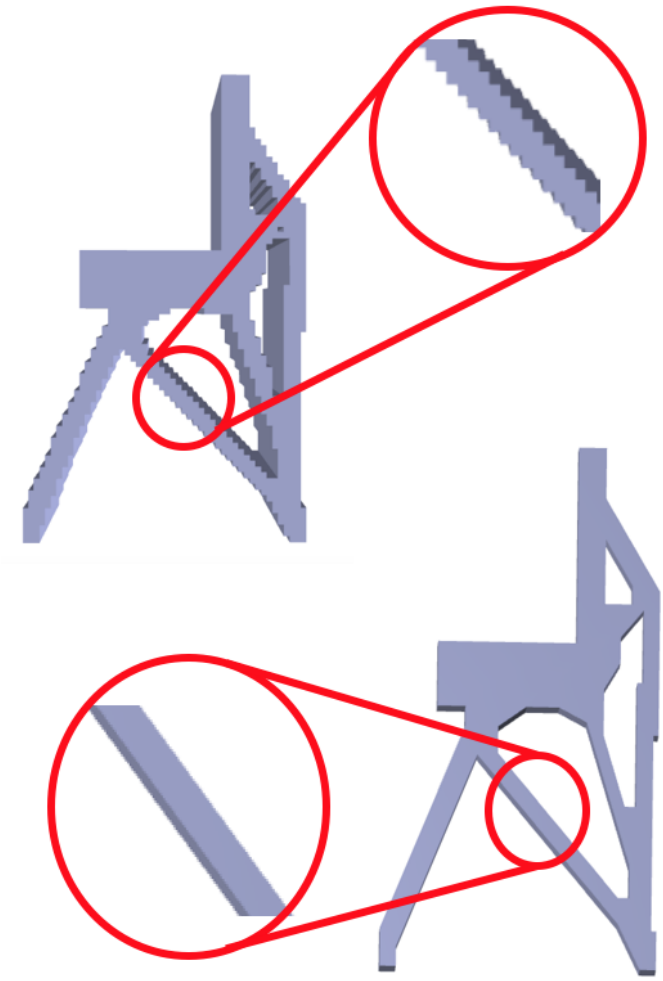

Figure 5.7 Every 0° overhang ≤ 0.2 mm (top) becomes a straight line (bottom). Longer overhangs are kept the same.

5.3.3 Simulation of the Modified Design Part

The numerical model developed for the first model has been applied for this model to predict critical areas of the design. All parameters and settings have been taken from the model before.

The deflection shown in Figure 5.11 are reduced compared to the simulation of deflection from the initial design. Y_{max} is, where inclined areas ≤ 0.2 mm, 0.9 mm. The maximum deflections are still noticeable at the larger 0° overhang surfaces below the seating area. After a chamfer and a pitch angle of 25° was applied, the simulation

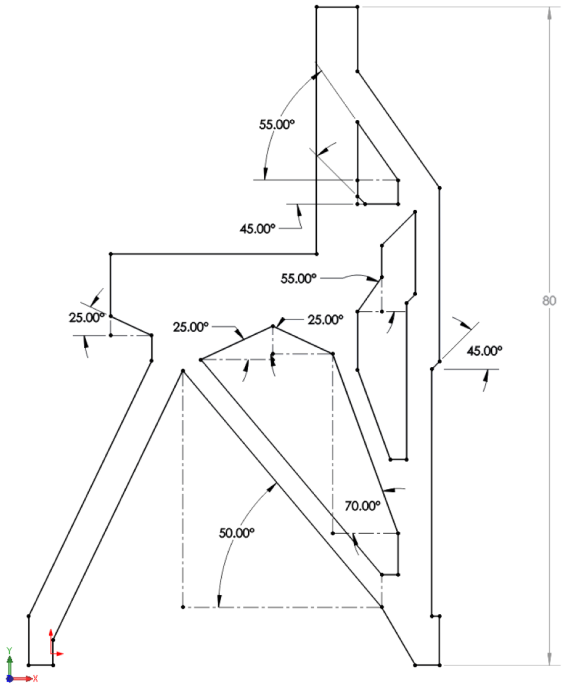

Figure 5.8 Design rules applied to the model with changing 0° overhangs ¿ 0.2 mm to a minimum of 25° overhangs as that has been shown as a steady angle for a smooth printing surface.

(Figure 5.12) of this design, predicted $y_{max} = 0.12$ mm, at the most conservative case. It can be said that support material will be neglectable and the printing surface will show now noticeable defects.

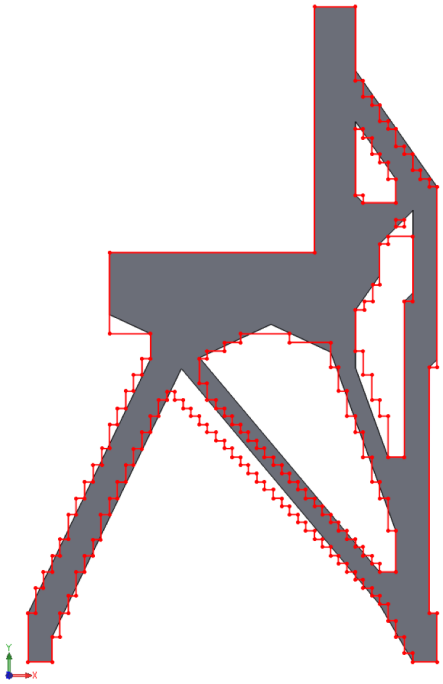

Figure 5.9 Design changes from the initial topology optimization design (red outline) with applied design rules (gray model).

5.3.4 3D Prints

The following section compares the numerical model to the physical prints of the chair design. Both designs (the low resolution TO design (TOD1) as well as the redesign (TOD2)) have been printed on the MakerBot. The default setting was used to print TOD1 with automatic generated support for overhangs. The result can be seen in Figure 5.13. Here the overhang length x_O is chosen to long and therefore the printer fully supports those 0° faces.

The post-processing of this part seems very difficult because the support material is in areas difficult to remove (breakthroughs). The support structure is a breakaway support at the MakerBot. Therefore, the surface after removing the support will show some defects. These defects do not diminish the print quality.

Figure 5.14 shows the same model (TOD1), printed without any support. This illustrates and also verifies the numerical model of maximum deflection. The numer-

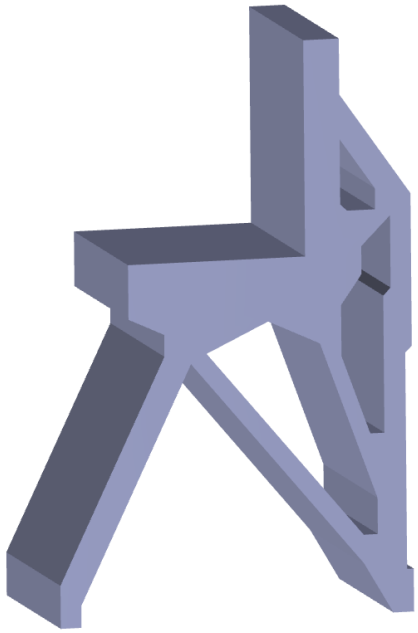

Figure 5.10 CAD model of the modified chair design to avoid 0° overhangs and minimal pitch angle.

ical model showed that the most deflection will appear at the overhang areas as well as the 0° faces. It can be seen on the printed model that the printed layers dripped down and created big defects on the surface. In the simulation y_{max} was determined with 1.2 mm and compared to the layer thickness of 0.3 mm that is 400% (detail view in Figure 5.15). The simulation is an over prediction, but clearly shows the predicted deflection compared to the printed real part.

After the design rules and founding of this research were applied to TOD1, TOD2 was printed. The simulation showed a very small deflection of $y_{max} = 0.12$ mm on the large overhang surface. Since there are no 0° faces left in the part, the deflection considered only the faces with a chamfer. As the simulation predicts a small deflection the printer will support in the default setting the minimum angle faces. The print has much less support as TOD1, see Figure 5.16. From previews results found by the numerical model and test specimens, TTOD2 can be printed without any support material with no noticeable defects on the overhang surface, see Figure 5.17 and 5.18.

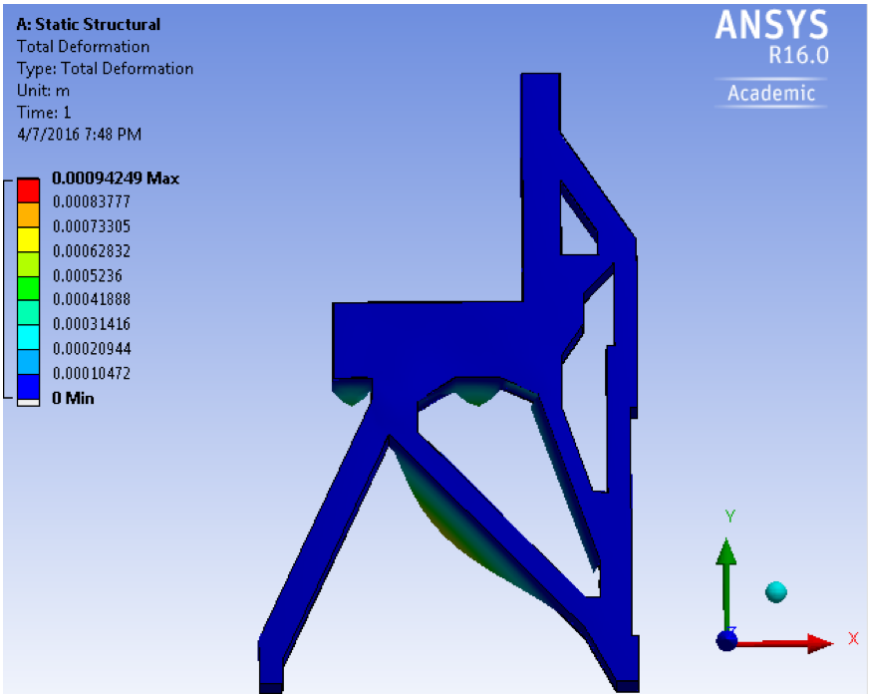

Figure 5.11 Simulation to predict the deflection of the topology optimized design with overhang ≤ 0.2 mm changes.$Y_{max} = 0.9$ mm.

With the physical experiments, the settings for the numerical model have been verified. Applying the design rules from this research helped to relinquish the support material and reduce printing time and material as well as removal of support material in inaccessible areas. Table 5.1 and 5.2 show the comparison between both prints subject to the printing time and material usage in both setting (with and without support).

Table 5.1 Comparison between TOD1 and TOD2 (no support) in terms of overall printing time and material usage.

	Print TOD1	Print TOD2
Printing time [h]	3.38	3.27
Model material [g]	82.01	76.49

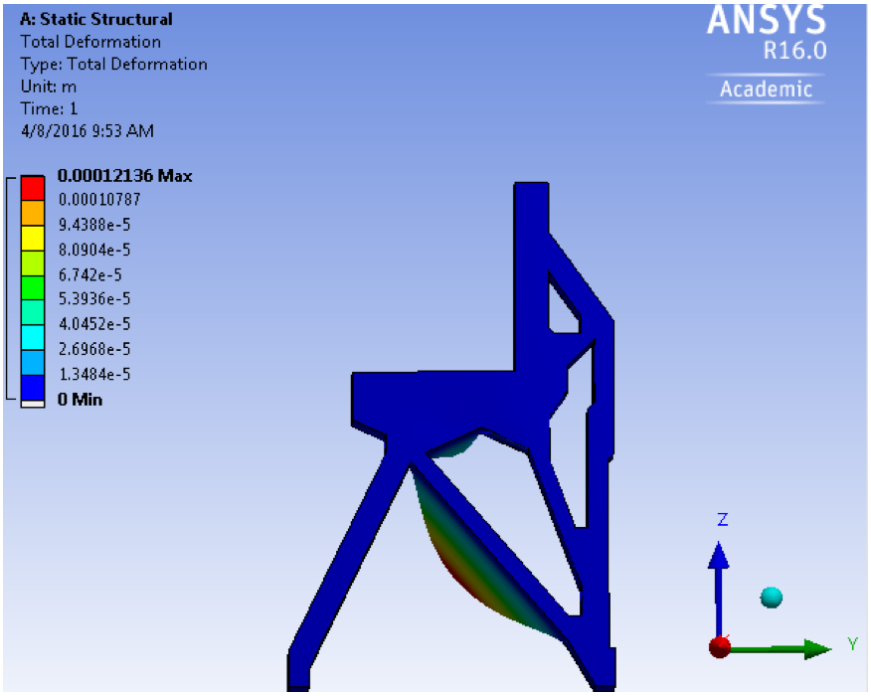

Figure 5.12 Simulation of the second modification with overhang ≤ 0.2 mm become a straight line and a chamfer and pitch angle of 25° have been applied. $Y_{max} = 0.12$ mm.

Table 5.2 Comparison between TOD1 and TOD2 (with support) in terms of overall printing time and material usage

	Print TOD1	Print TOD2
Printing time [h]	5.25	3.51
Model material [g]	82.01	76.49
Support Material [g]	50.32	11.69

5.4 Results

This experimental study of deflection prediction with a numerical model in FDM printing revealed challenges and issues for FDM, apparent on complex, large scale models. The effect of different factors to determine the deflection was simulated and studied with this approach. The parameters that influence the deflection where also visible in the simulations by using established parameters of the thermoplastic. The result shows that a conservative simulation, by using a low Young's modulus at a high

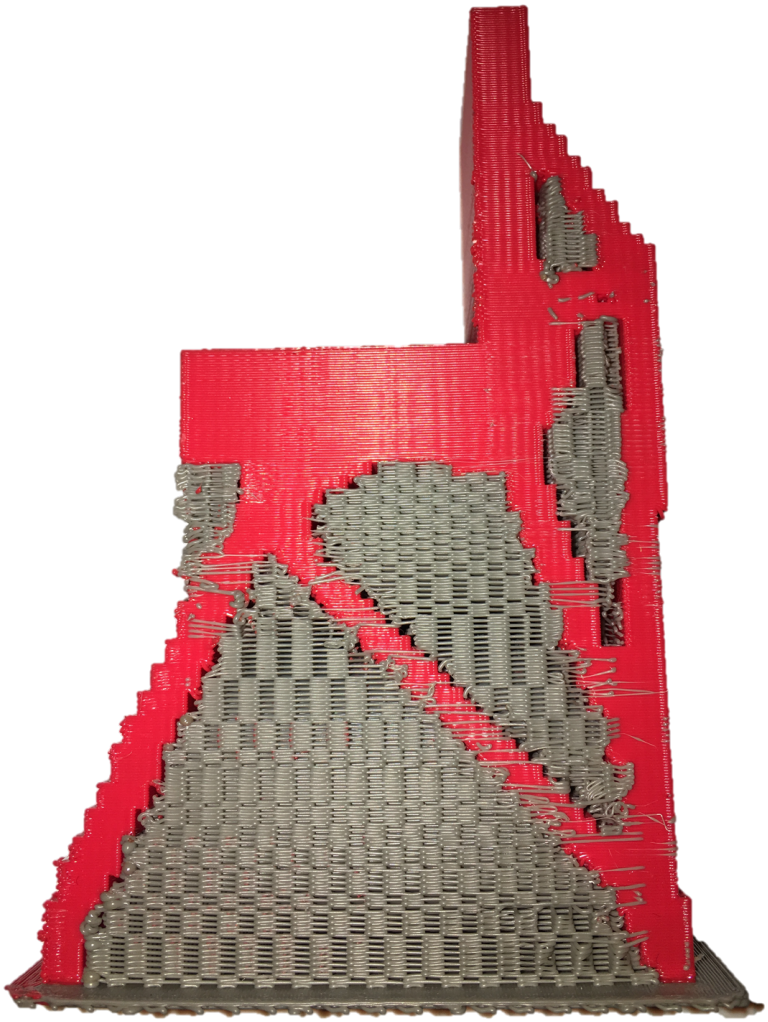

Figure 5.13 Initial design printed with default settings and full support structure.

simulation temperature, can be predicted and matched with an experimental print. Even though the actual change of temperature in the model is not simulated, the over prediction helps to see where difficult areas are and support structure needed.

Dr. Tovar's topology optimization application for MATLAB develops an optimized model of an initial design idea while maintaining the same stiffness for defined load cases. The case study has shown that a direct implementation from the application into a finite element software, will give a surface structure with many 0° overhangs and an undefined length. This also is the outcome of a low-resolution

Figure 5.14 TOD1 printed without any support structure.

image. To compare the simulation with the 3D prints, a model has been printed. The prediction via simulations had been confirmed at the problematic areas form the simulations at the print. The dripping and surface defects are as simulated on the overhangs and small chamfer angels.

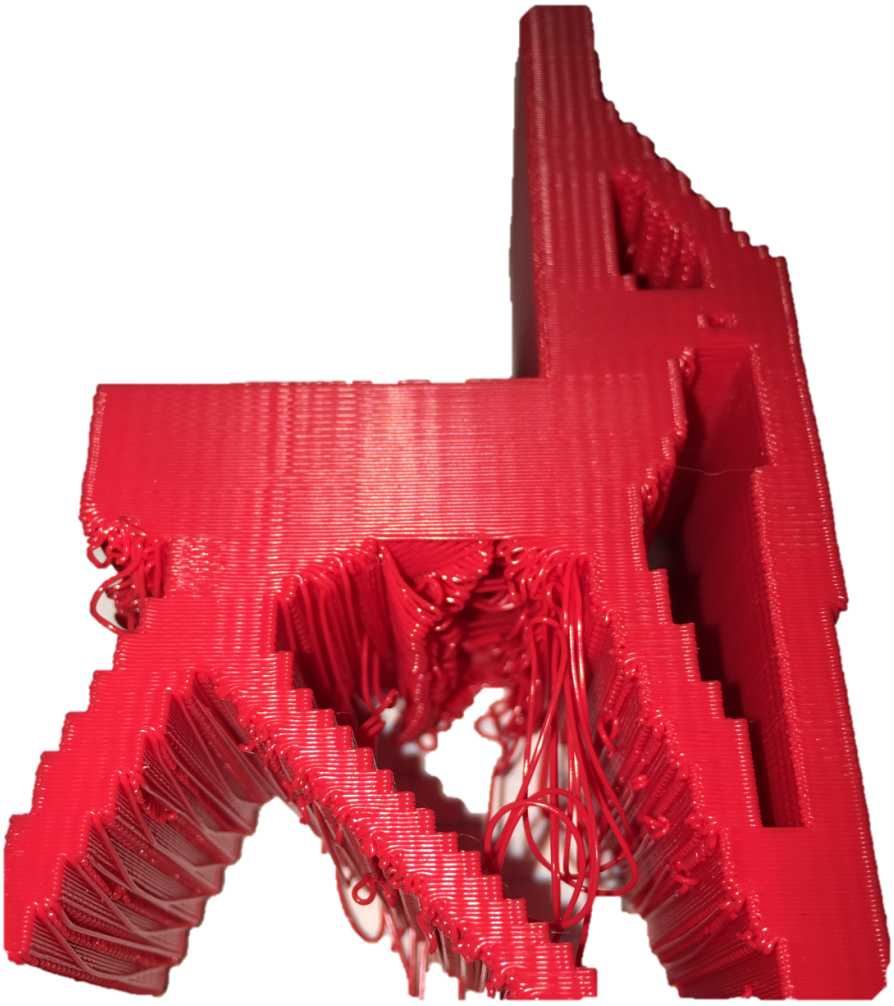

Figure 5.15 Detail view of TOD1 showing the deflection from single layers as predicted in the numerical model.

To achieve the goal of minimizing the support, the design was changed to earlier developed overhang length x_O with a maximal length of 742 μm and a minimum angle α of 22°. The new re-designed model has shown, after simulations, there are still areas of deflection at the down faced surfaces but it is so small that it can be

Figure 5.16 TOD2 print with default setting for support structure.

neglected. After printing the design, the prediction has matched with the result of the print. The model was able to print without support and no defects where noticed. The principle of the layer-by-layer technology will lead to a drip at the end of a layer if it is on an increasing angle. The simulations within this case study have shown that

Figure 5.17 TOD2 printed without any support structure.

changing the design will minimize the deflection. In addition, using the worst case scenario of parameters, high temperature and low effective modulus, an equivalent conservative numerical model can be created.

Figure 5.18 Detail view of TOD2.

6. SUMMARY, CONCLUSION AND FINAL REMARKS

6.1 Summary

This research work presents the analytic, experimental, as well as numerical foundation for a new design approach for self-supported structures using the fused deposition molding (FDM) method. Minimizing the support structure is achieved in two ways: part positioning or part design modification. Both criteria had been evaluated within the Selective Laser Melting (SLM) process as it is reviewed in Chapter 1. For FDM, it rarely has been researched and the development of a numerical model was developed to predict critical surface areas require support.

Analytic Model: With the way material is extruded at the FDM process, layer-by-layer, the work is based on a investigation about a variety of linear beam deflections. A linear model was considered for simplification and representation of the deflection for FDM printed parts. The theory from Euler-Bernoulli was compared to Timoshenko's beam theory. Since the Euler-Bernoulli beam theory showed an analytical deviation in deflection from physical printed parts, Timoshenko's beam theory was more applicable. This theory had to be modified according to the large length-diameter ratio where the shear coefficient needs to be considered. By using the modified beam theory for micro-structures, the analytic model can predict the deformation of the filament after extrusion in the FDM process. It is calibrated based on experimental observations of the deflection in multiple 3D print test models. The resulting constitutive equation is used in a numerical finite element analysis model.

Physical Tests with corresponding numerical models: Since the building process at extrusion is simulated, material properties at this point of time have not been investigated. ABS for FDM is in his initial state is solid. During the print it

melts in the heated nozzle before it gets extruded on the printing platform. The behavior of melted ABS is viscous material and a effective modulus has to be computed for linear deflection. Through a deformation experiment print, the effective modulus was developed at the point of extrusion and with the before established analytic model computed. This parameter has been implemented into the numerical model for further simulations.

Single strand experiments: are developed to find a temperature dependent Young's modulus from 200°C up to 245°C. The result was as expected, the single printed strand had the highest deflection at 245°C with 589 μm and the smallest at 200°C with 64 μm. Based on the information from the analytic model and the Timoshenko's modified beam theory. As a result the effective modulus is decreasing from 9.53 GPa at 200°C to 1.03 GPa at 245°C.

Pitch angle: experiments were based on the default printing angle setting of 45°. By printing a chamfer with this angle an overhang of 0.165 mm could be detected. Simulations of chamfers with α from 15° up to 60° had shown a major variance of deflection at the tip of each layer. The numerical model predicted a deflection of about 200% from the layer thickness of 300 microns at a chamfer of 15°, which is equal to 0.598 mm. Furthermore, all simulations confirmed the measurements compared to the physical prints with a chamfer of 15°, 20°, 30°, 45° and 60°. The simulations were realized with a constant effective modulus of $E = 1.91$ GPa at a constant temperature of 225°C, which is the extrusion temperature of the MakerBot. As a founding of the simulation with verification of physical prints it can be found out that using a 5% deflection offset, the overhang angle can be reduced to about 22° to 27°, with 200μm $\leq x_o \leq$ 315μm at a printing diameter of 300 microns.

Circular specimen: (where support structures are unavoidable) were printed and analyzed next. The default setting of the 3D FDM printer fully supports the 0° overhang and it is very difficult to remove the support material in the post-process at

inner structures without noticeable marks. The need for a design change to minimize or relinquish support structure is needed. Simulations have shown that the most problematic area of this geometry is like expected the 0° overhang. With an increasing hole diameter, the defects worsens. The prints where acceptable for a hole less than 5 mm. Above 5 mm, all prints failed. As a result, the model has been changed to a hole with a additional tangential tip, with a slope of 15°. This was taken over from previous results and with a small overhang angle the design change does not exceed the overall diameter to much. This time the numerical model has shown the highest deformation at a hole diameter of 7 mm and a tip height of 0.5 mm. As the geometry increases the surface of the overhang gets smoother and the deflection decreases, as the simulations predicted.

As the geometry gets more complex, all parameters, i.e., the environmental temperature, the temperature profile at the part from the heated printing platform up to the cooled down layer, the chamber temperature (if its an enclosed system) have to be considered. This is why the numerical model is simulating the parts at a higher temperature (245°C) than it is actual used for printing and $E = 1.04$ GPa. By this way a more conservative prediction is achievable. This means, it will over predict the behavior of the part during the print and will point out the critical surface areas where support is needed or design changes are necessary. It can be said that these physics-based numerical models are fundamental to the design of support structures and self-supported 3D printed components. All findings are displayed and summarized in Figure 6.1 as well as in Table 6.1 below:

Case Study: In the last part of this research a case study has been used to show the usage of the simulation model in comparison with a topology optimization application, developed by Dr. Tovar. The study is based on a chair design; which topology was optimized by Dr. Tovar's MATLAB GUI. After applying two load cases, a person is sitting on the chair (LC1) and is also leaning back (LC2) the 100% support underneath the chair was optimized to a volume of 30%. This final design was modeled

Table 6.1 Design rules for aggregated structures: Overhang-length; pitch angle, Fillets, merged design

Overhang-length x_O	Short enough to ensure manufacturability, best overhang-length 0.2 mm $\leq x_0 \leq$ 0.32 mm, at a5% threshold.
Pitch angle	Models should be oriented orthogonally to the printing platform to avoid any support if not possible inclined areas with a pitch angle $22° \leq \alpha \leq 27°$ will be printable without support.
Hole, Fillets	Holes or fillets require support if the diameter is >10 mm. If diameter $h_d \leq 10$ mm no support is required.
Merged Design (α, x_O, r_i)	Inner surface gets better with an increasing hole diameter, $h_d \geq 10$ mm and $tip_h \geq 0.7$ mm.

and analyzed with the developed numerical model. An over prediction was also used for this simulation to see how the model will deform without support structures. The simulation showed clearly all surfaces, which have an overhang smaller than 45° needed to be re-designed for printing without support. Running simulations with a changed design, applying the design rules of the overhang angle and no 0° overhangs, (forming a tip), showed that the chair has minimized the deflection of the overhang to a maximum of 0.16 mm, which is negligible, compared to a deflection of 1.2 mm at a layer thickness of 300 microns. To verify the simulation, both designs have been printed and it has shown that the numerical model over predicted the deformation at the correct areas where they occurred at the physical print.

6.2 Conclusion

Multiple prints and experiments have proven that Euler-Bernoulli's beam theory and the general equation for beam deflection is not applicable to the problem faced in

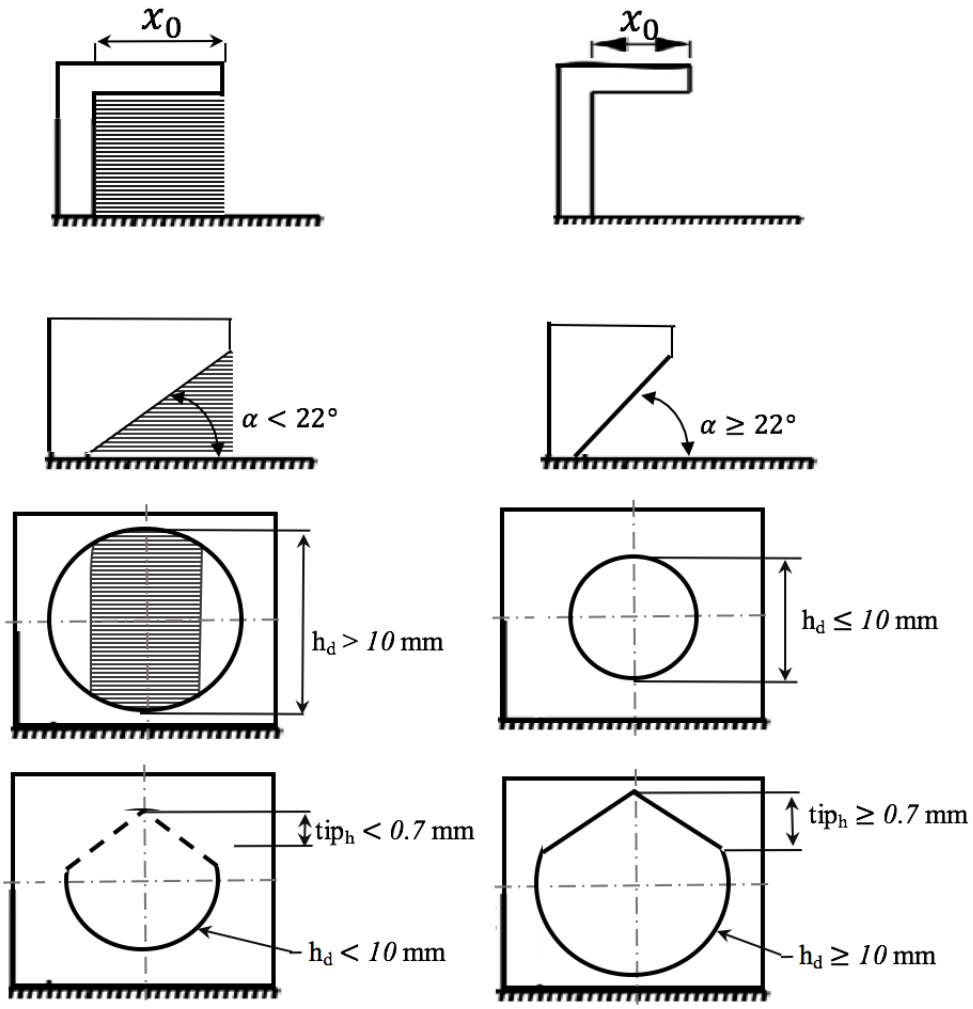

Figure 6.1 Overview of analyzed aggregated structures with corresponding design rules. From the top: Overhang-length, pitch angle, Holes, merged design

this work. For determining material properties of 3D printed parts within the FDM process, Timoshenko's modified beam theory for micro structures was more precisely. By using this theory, an effective modulus of ABS could be determined at the time of filament extrusion with a variety of physical tests. Based on this information, a prediction of deformation with a numerical model for different printed part features, was developed. In this research, design rules were established beyond current rules [8, 14] for DfAM and FDM, which help to minimize the support structure. In addition to the independent research of different geometries and features, the collaboration be-

tween AM and topology optimization was extended by manual applying the design rules. The study of a complex component showed that with the computed material properties a conservative numerical model (high temperature and low effective modulus),support material can be reduced by about 75%, in this particular case.

6.3 Final Remarks

The numerical model and material behavior of ABS observed during this study focused on prediction of 3D printed parts and the deformation of overhang surface areas. With the analytic model, an effective modulus can be computed. This information permits numerical model adjustment. The temperature profile was not considered during simulation. The part has different temperature zones and those influence the deflection. Suggestions for further studies seem relevant and the following ideas could carry on this research:

a)Numerical model for multiple material use: The analytic model can be extended to compute a dynamic modulus with viscous-elasticity E^* for a real simulation of each printed layer with multiple materials. In this research the only material which has been considered was ABS. With a general computation of a dynamic modulus, different material can be chosen and applied to the numerical model and analyzed.

b) Thermal profile of the part: The numerical model can be extended to incorporate the different thermal zones, which occur in the part. Zone one would be the temperature profile from the heated printing platform to the printed layer. This temperature is in the most cases below the extrusion temperature and while each layer is printed at about 225°C the part is heated up from below with about 110°C. Zone two is the extrusion temperature and is a transition zone from a lower temperature from the bottom to the highest temperature with a viscus material behavior up to the cooling zone. Zone three appears after the part cools down and this is time dependent

and depends for example on how many cooling fans are being used (see Figure 6.2). Those variables need to be implemented in the numerical model, to have a more specif model and less a conservative over prediction of the deformation.

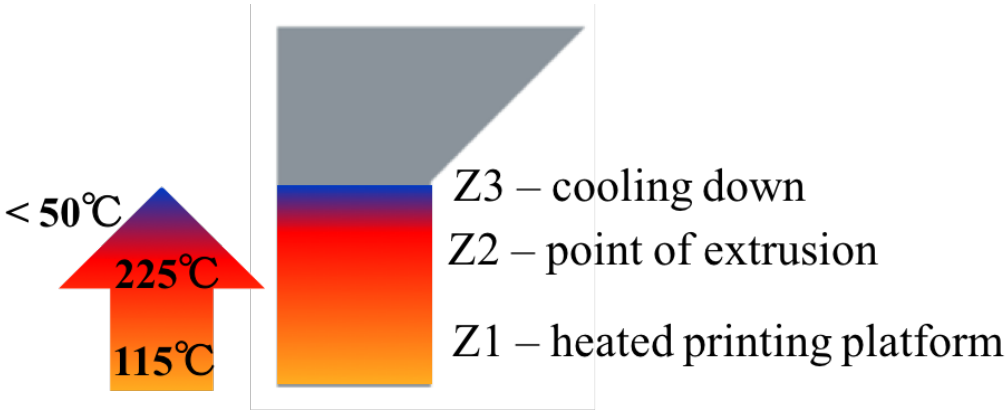

Figure 6.2 Thermal profile of a 3D printed part at the FDM process. Zone1: heating platform; Zone2: extrusion temperature; Zone3 cooling

c) Automatic threshold checkup: For further help of improving the support structure an automatic threshold setup can be developed which helps the user to identify critical areas and angles faster. It can be an application in MATLAB, where the STL-file can be imported and used for measurements. This application needs to then be linked with the numerical model for analysis. As a result the optimized STL-file is able to print with reduced support structure on any FDM printer

c) Topology optimization extension with developed design rules: The threshold of angles and overhangs can be controlled automatically within the MATLAB GUI from Dr. Tovar. This will lead to cooperation between the topology optimization tool and the design rules developed in this research. During the optimization process the application will control the design space and cross-check the threshold with the optimized design and re-calculates the structure, for example if the angle of a slope is not blow 25°, to keep the same behavior, such as stiffness of the part.

d) Prevention of warping: If the 3D printed part is solid and the dimensions are unproportional of height to length, the FDM printer will add a raft below the model. The raft is about two layer thick and remains underneath the complete part. We could see at multiple experiments, that the part including the raft will warp after cooling down. This is caused by shrinking of the part. A future solution would be to split the part in multiple sections (Figure 6.3) to take out the thermal stress in the raft and relax the tension on the part. This also can be simulated and test within a extension of the numerical model.

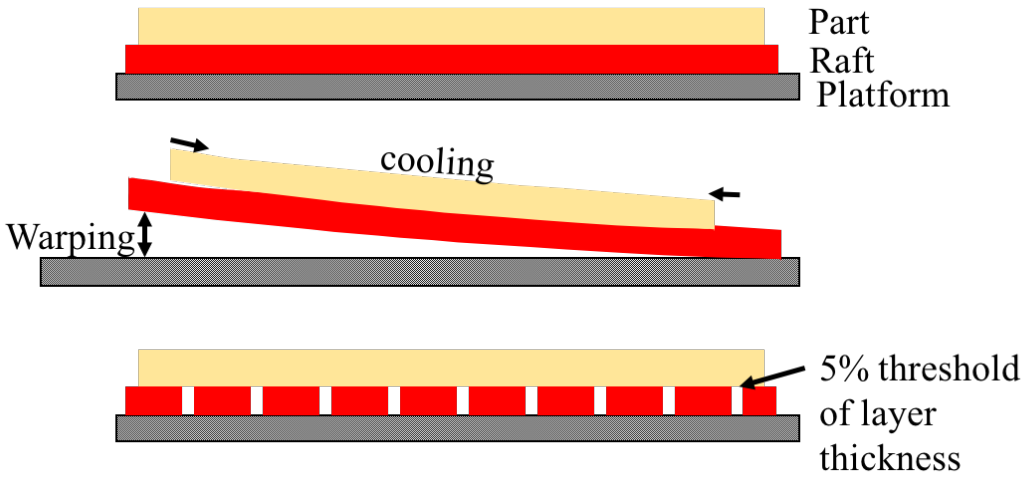

Figure 6.3 Dividing the raft underneath a solid part to take out the thermal stress.

LIST OF REFERENCES

LIST OF REFERENCES

[1] J. Faludi, C. Bayley, S. Bhogal, and M. Iribarne. Comparing environmental impacts of additive manufacturing vs traditional machining via life-cycle assessment. *Rapid Prototyping*, 21:14–33, 2015.

[2] G. Strano, L. Hao, R. M. Everson, and K. E. Evans. A new approach to the design and optimisation of support structures in additive manufacturing. *International Journal of Advanced Manufacturing Technology*, 66(9-12):1247–1254, 2013.

[3] B. Ezair, F. Massarwi, and G. Elber. Orientation analysis of 3D objects toward minimal support volume in 3D-printing. *Computers & Graphics*, 51:117–124, 2015.

[4] S. Naghieh, M.R. Karamooz Ravari, M. Badrossamay, E. Foroozmehr, and M. Kadkhodaei. Numerical investigation of t he mechanical properties of the additive manufactured bone scaffolds fabricated by fdm: The effect of layer penetration and post-heating. *Journal of the Mechanical Behavior of Biomedical Materials*, 59:241 – 250, 2016.

[5] Z. Doubrovski, J. C. Verlinden, and J. M. P. Geraedts. Optimal design for additive manufacturing: Opportunities and challenges. In *Proceedings of the ASME Design Engineering Technical Conference*, volume 9, pages 635–646, 2011.

[6] O.J. Horger, S.L. Hoyt, J.W. Huckert, and R.W. Bolz. *ASME Handbook Material Engineering: processes*. 1958.

[7] D. W. Rosen. Design for additive manufacturing: A method to explore unexplored regions of the design space. *18th Solid Freeform Fabrication Symposium, SFF 2007*, pages 402–415, 2007.

[8] G. Adam and D. Zimmer. Design for Additive Manufacturing-Element transitions and aggregated structures. *CIRP Journal of Manufacturing Science and Technology*, 7(1):20–28, 2014.

[9] B. Vayre, F. Vignat, and F. Villeneuve. Designing for additive manufacturing. In *Procedia CIRP*, volume 3, pages 632–637, 2012.

[10] R. Ponche, J. Y. Hascoet, O. Kerbrat, and P. Mognol. A new global approach to design for additive manufacturing: A method to obtain a design that meets specifications while optimizing a given additive manufacturing process is presented in this paper. *Virtual and Physical Prototyping*, 7(2):93–105, 2012.

[11] N. Gardan and A. Schneider. Topological optimization of internal patterns and support in additive manufacturing. *Journal of Manufacturing Systems*, 37:417–425, 2015.

[12] P. S. Chang and D. W. Rosen. The size matching and scaling method: A synthesis method for the design of mesoscale cellular structures. *Proceedings - 2010 International Conference on Manufacturing Automation, ICMA 2010*, pages 79 – 86, 2010.

[13] D. W. Rosen. Research supporting principles for design for additive manufacturing: This paper provides a comprehensive review on current design principles and strategies for am. *Virtual and Physical Prototyping*, 9(4):225 – 232, 2014.

[14] G. Adam and D. Zimmer. On design for additive manufacturing: Evaluating geometrical limitations. *Rapid Prototyping Journal*, 21(6):662–670, 2015.

[15] D. Thomas. *The Development of Design Rules for Selective Laser Melting (Doctoral dissertation)*. University of Wales, Institute, Cardiff, 2009.

[16] W. K. Brooks, J. Todd, and C. J. Sutcliffe. Automatic lattice geometry generation for rapid manufacture. pages 19–25. 6th National Conference on Rapid Design and Manufacture, Buckinghamshire, 2005.

[17] B. Vandenbroucke and J. P. Kruth. Selective laser melting of biocompatible metals for rapid manufacturing medical parts. volume Rapid Prototyping Journal 13 (4), pages 196–203. Rapid Prototyping Journal 13, 2007.

[18] G. Hodgson, A. Ranellucci, and J. Moe. Slic3r Manual – Support Material. slicer.org), 2016.

[19] AlphaSTAR GENOA FEA Software for 3D printing; http://innovationintelligence.com/worlds-first-drivable-3d-printed-automobile/; (last accessed April 2016).

[20] B. Wang, J. Zhao, and S. Zhou. A micro scale Timoshenko beam model based on strain gradient elasticity theory. *European Journal of Mechanics, A/Solids*, 29(4):591–599, 2010.

[21] K. Liu and A. Tovar. An efficient 3D topology optimization code written in Matlab. *Structural and Multidisciplinary Optimization*, 50(6):1175–1196, 2014.

[22] S. S. Crump. US Patent - Apparaturs and methof for creating three-dimensional object, 1989.

[23] I. Gibson, D. W. Rosen, and B. Stucker. *Additive Manufacturing Technologies*. 2010.

[24] Q. Sun, G.M. Rizvi, C.T. Bellehumeur, and P. Gu. Effect of processing conditions on the bonding quality of FDM polymer filaments. *Rapid Prototyping Journal*, 14(2):72–80, 2008.

[25] B. N. Turner, R. Strong, and S. A. Gold. A review of melt extrusion additive manufacturing processes: I. Process design and modeling. *Rapid Prototyping Journal*, 20(3):192–204, 2014.

[26] M. A. Yardimci and S. Güçeri. Conceptual framework for the thermal process modelling of fused deposition. *Rapid Prototyping Journal*, 2(2):26–31, 1996.

[27] C. M. Wang. Timoshenko Beam-Bending Solutions in Terms of Euler-Bernoulli Solutions, 1995.

[28] R. Budynas and K. Nisbett. *Shigley's Mechanical Engineering Design, SI Version*. 2009.

[29] Bbanerje; http://habituatingfea.blogspot.com/2012/11/thin beam-vs-thick-beam.html; (last accessed December 2015).

[30] B. Zindler. Kleiner Ausflug in die Balkentheorie– Die Durchbiegung w als zentrales Element. www.Zenithpoint.de, 2016.

[31] MakerBot Replicator 2X; https://makerbotshop.com.au/sites/default/files/replicator-2x(last accessed January 2016).

[32] Plugin digital Microscope 2016; http://www.amazon.com/Plugable-Microscope-Flexible-Observation-Magnification/dp/B00XNYXQHE; (last accessed January 2016).

[33] T. Kaneko. On Timoshenko's correction for shear in vibrating beams. *Journal of Physics D Applied Physics*, 8, 1975.